2007-07-16

Microfacies Analysis, Sedimentary Petrology, and Reservoir Characterization of the Sinbad Limestone Based Upon Surface Exposures in the San Rafael Swell, Utah

Caleb R. Osborn
Brigham Young University - Provo

MICROFACIES ANALYSIS, SEDIMENTARY PETROLOGY, AND RESERVOIR CHARACTERIZATION OF THE LOWER TRIASSIC SINBAD LIMESTONE MEMBER OF THE MOENKOPI FORMATION BASED UPON SURFACE EXPOSURES IN THE SAN RAFAEL SWELL, UTAH.

by

Caleb R. Osborn

A thesis submitted to the faculty of

Brigham Young University

In partial fulfillment of the requirements for the degree of

Master of Science

Department of Geology

Brigham Young University

August 2007

BRIGHAM YOUNG UNIVERSITY

GRADUATE COMMITTEE APPROVAL

of a thesis submitted by

Caleb R. Osborn

Each member of the following graduate committee has read this thesis and by majority vote has been found to be satisfactory.

_____	_____
Date	Scott M. Ritter, Committee Chair
_____	_____
Date	Thomas H. Morris
_____	_____
Date	Brooks B. Britt

BRIGHAM YOUNG UNIVERSITY

As chair of the candidate's graduate committee, I have read the thesis of Caleb R. Osborn in its final form and have found that (1) its format, citations, and bibliographical style are consistent and acceptable and fulfill university and department style requirements; (2) its illustrative materials including figures, tables, and charts are in place, and (3) the final manuscript is satisfactory to the graduate committee and it is ready for submission to the university library.

_____ _____

Date

Scott M. Ritter
Chair, Graduate Committee

Accepted for the Department

_____

Dr. Michael J. Dorais
Graduate Coordinator

Accepted for the College

_____

Thomas W. Sederberg
Associate Dean, College of Physical and Mathematical Sciences

ABSTRACT

MICROFACIES ANALYSIS, SEDIMENTARY PETROLOGY, AND RESERVOIR CHARACTERIZATION OF THE LOWER TRIASSIC SINBAD LIMESTONE MEMBER OF THE MOENKOPI FORMATION BASED UPON SURFACE EXPOSURES IN THE SAN RAFAEL SWELL, UTAH.

Caleb R. Osborn

Department of Geology

Master of Science

The Lower Triassic Sinbad Limestone Member of the Moenkopi Formation has produced minor amounts of oil in the Grassy Trail Creek field near Green River, Utah and is present below much of central Utah including the recently discovered Covenant field. Superb outcrops of this thin (15 m), mixed carbonate-silicilastic unit in the San Rafael Swell permit detailed analysis of its vertical and lateral reservoir heterogeneity. Vertically, the Sinbad Limestone comprises three facies associations: (A) a basal storm-dominated, well-circulated skeletal-oolitic-peloidal limestone association, (B) a storm-dominated, poorly-circulated hummocky cross-stratified siliciclastic/peloidal association,

and (C) a capping peritidal cross-bedded oolitic dolograinstone association. Eleven microfacies are present in 14 measured sections within the Sinbad Limestone. Lateral variation is most pronounced in the upper part of the basal limestone where storm-deposited beds pinch out over a lateral distance of one kilometer. Otherwise, individual beds and microfacies display a large degree of lateral homogeneity and regional persistence.

Diagenesis is strongly controlled by microfacies. Diagenetic elements include marine fibrous calcite cements, micritized grains, compaction, dissolution and neomorphism of aragonite grains, meteoric cements, pressure dissolution, and dolomitization. The paragenetic sequence progresses from marine to meteoric to burial. Marine and meteoric cements occlude much of the depositional porosity.

Hydrocarbon-lined interparticle and separate vug (largely molds) pores (1-5%) characterize the skeletal-oolitic limestones with permeability ranging from 0-100 md. Low permeability/porosity characterizes the middle silicilastic unit. The best reservoir qualities (permeability 400 md) occur in portions of the dolomitized oolitic grainstones that form the upper 2 to 3 m of the Sinbad Limestone.

Fracture analysis of the studied area indicates a strong NW-SE trend. Fracture spacing is associated with lithology. Fracturing of limestone possibly displays a higher dependence upon bed thickness and microfacies type. The degree of dolomitization controls and increases fracture spacing while siltstones display more closely spaced fractures.

The basal limestone unit is an oil storage unit, medial siltstones are flow baffles/barriers, and the dolostone caprock is an oil flow unit. If good connectivity

through fractures can be obtained between the dolostone and limestone units, the Sinbad Limestone has potential to serve as a reservoir. This study will not only aid in future Sinbad exploration, but will serve as a model for parasequence-scale intervals in thicker mixed carbonate-siliciclastic successions.

ACKNOWLEDGEMENTS

I would like to express appreciation to Dr. Scott M. Ritter for his inspiration, as well as sharing his time, knowledge, and insights. I appreciate all of the professors who have provided me with glances into the many subdisciplines of geology and have inspired me in many ways. I express thanks to Dr. Eric Christensen for the use of his hand held scintollometer, Dr. Tom Morris, Dr. Brooks Britt and Randy Skinner for their encouragement. I would also like to thank the Department of Geology office secretaries, including Kris Mortensen, Marge Morgan, and Kim Sullivan for the help and knowledge that they selflessly provided me. I acknowledge Ashley Dalrymple, Teagan Tomlin and Riley Brinkerhoff for help with Adobe Illustrator and John Yeade and Drew Derenthal for working and providing information to me in the field and lab. I would also like to thank field camp students from 2006 who provided me with stratigraphic columns and information about the area. I offer my sincere thanks to all of my family members and my wife's family members as well. Finally, I would like to thank my wife and son for their encouragement toward helping me succeed in my endeavors. Without them, this thesis would have been impossible.

TABLE OF CONTENTS

INTRODUCTION

The Lower Triassic Sinbad Limestone Member of the Moenkopi Formation has produced small quantities of oil from the Grassy Trail Creek Field located northwest of Green River, Utah (Figure 1) and is present in the subsurface throughout much of central Utah, including beneath the recently discovered Covenant field. The Sinbad is faulted to depths of over 3000 m along the Utah hingeline. Dean (1981) reported excellent subsurface oil shows from the Sinbad in Sanpete County and along the Wasatch Plateau. Although its relative thinness precludes it from being a major producer of oil, the Sinbad Limestone does bear potential for modest future oil production. Such production will require a sound understanding of the vertical and lateral heterogeneity of the Sinbad Limestone in the context of its depositional, diagenetic, and structural (fracture) history.

In the San Rafael Swell, Utah, (Figure 1), the Sinbad is extensively exposed on low mesas ranging in size from approximately 0.4 to 2.0 square miles. Outcrop is continuous to nearly continuous around the perimeters of these mesas. Widespread exposure of the Sinbad Limestone in these areas permits 1) the development of a depositional model for this mixed, shallow-marine carbonate-siliciclastic system, 2) the determination of the nature and timing of depositional, diagenetic, and structural processes controlling the distribution of permeability and porosity, and 3) the characterization of the vertical and lateral heterogeneity of the Sinbad Limestone. Data from the San Rafael Swell can be used to develop an outcrop analog for the Sinbad Limestone in the nearby Grassy Trail Creek Field (located 100 km due north) and potential future Sinbad plays. Though narrowly focused on the Sinbad Limestone, results

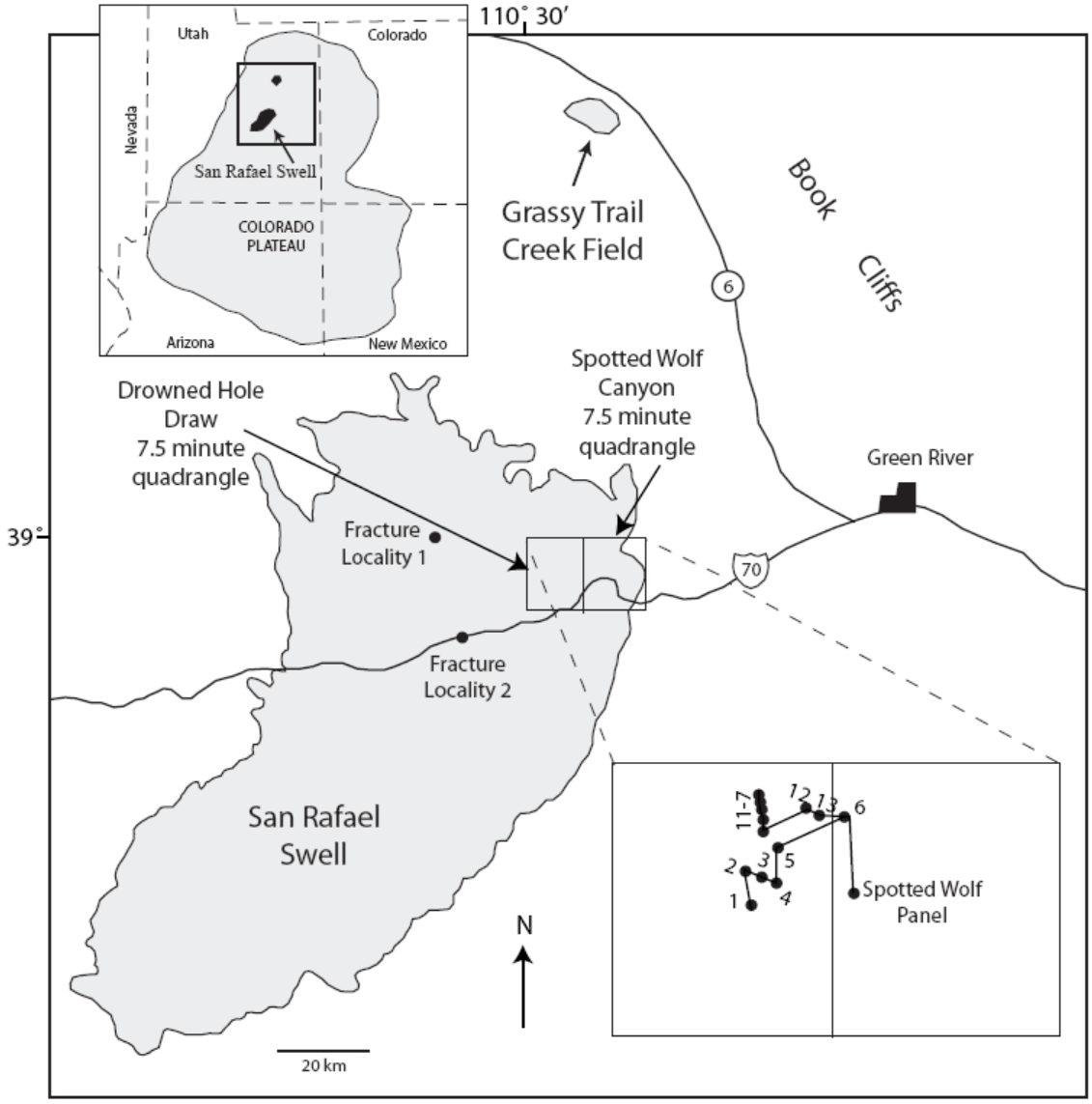

Figure 1. Location of study area showing the Grassy Trail Creek field, measured sections, correlation lines, and fracture localities. See Appendix for more detailed locations of the measured sections.

from this study will increase our ability to model the behavior of thin, mixed carbonate-siliciclastic flow/storage intervals (i.e. mixed-lithology parasequences) that form components of larger reservoir volumes.

PREVIOUS WORK

The Sinbad Limestone Member of the Moenkopi Formation was named by Gilluly and Reeside (1928) for relatively thin (15 to 25 meters) mesa-capping carbonates

exposed in the crest ("Sinbad Country") of the San Rafael Swell, central Utah (Figure 1). The Sinbad was subsequently traced westward to the flanks of the Henry Mountains where Hunt (1953) recovered Early Triassic ammonoids. During the 1960's, the Sinbad Limestone was mentioned only briefly in reports on the uranium potential and mineralogy of the Moenkopi Formation by Smith et al. (1963) and Hawley et al. (1968), respectively. The regional distribution and depositional environments of the Sinbad were described by Stewart et al. (1972) as part of their study of the Moenkopi Formation. In his more detailed studies of the Moenkopi in southeastern Utah, Blakey (1973a and b) and (1974) developed an informal tripartite (basal limestone- middle silty calcilutite-sandy dolostone cap) subdivision of the tidally-dominated Sinbad Limestone. Dean (1981) studied the depositional and diagenetic environments of the Sinbad in the Teasdale Dome located in and around Capitol Reef National Park, Utah. Batten and Stokes (1986) examined the numerous species of gastropods found in this member in exposures in the San Rafael Swell, Utah. During the 1990's a few abstracts (Porter, 1991, Lutz, 1993, and Goodspeed and Elrick, 1993) discussed the sequence stratigraphy of the Sinbad Limestone specifically and the Moenkopi Formation in general. The Sinbad has received little attention since then, except for paleontological studies by Schubert and Bottjer (1995), Twichett et al. (1995), Fraiser and Bottjer (2000, 2004), Boyer et al. (2004), Nutzel and Schulbert (2005), Hautmann and Nutzel (2005), and the subsurface studies cited below.

The Sinbad Limestone produced oil from a 445 foot-long lateral in the Grassy Trail Creek located on the north-plunging nose of the San Rafael Swell (Figure 1). Lutz and Allison (1992) identified two carbonate lithofacies in core: cross-bedded oolite and

skeletal wackestone to packstone. Oolitic shoal sands (up to 8 meters thick) contain minor intraparticle porosity related to preferential dolomitization of ooids and intergranular (interooid) porosities of 10%. Measured permeability ranges between 0.52 to 0.88 md with 20% oil saturation (Lutz and Allison, 1992; Allison et al., 1993). Skeletal wackestones and packstones have measured porosities of 1 to 2% and permeabilities ranging from 0.01 to 0.02 md.

Gas flows of 15 to 30 MMCF were encountered in the Sinbad Limestone between 2,725 and 2,755 feet in the Last Chance South field located on the southwestern flank of the San Rafael Swell in southwestern Emery County, Utah (Jackson, 1993). In their summary of oil and gas exploration in Carbon, Emery, and Sanpete Counties, Laine and Staley (1991) listed evaluation of the Moenkopi reservoirs using horizontal drilling techniques as a recommended target for future exploratory efforts.

METHODS

To meet the objectives discussed above, 14 standard stratigraphic sections were measured in the Drowned Hole Draw and Spotted Wolf Canyon 7.5 minute quadrangles (Fig. 1). Sections were spaced to emulate the 40 to 80 acre spacing typical of many oil fields. Gamma ray data were collected from these sections using a hand-held Scintrex GRS-500 scintollometer. Representative samples of each bed within sections 1, 4, 6, 7, and within the Spotted Wolf section (a total of 89 samples) were impregnated with blue epoxy and thin-sectioned for detailed petrographic analysis using a Nikon Eclipse 6400POL petrographic microscope. Oriented rock samples were described and classified according to Dunham (1962), Dott (1964), and Lucia (1995). Relative abundances of skeletal grains, non-skeletal grains, mud, and diagenetic components (porosity percent

and types, cement, etc.) were determined for each thin section. Abundance data were used for statistical calculation of microfacies using Paleontological Statistics (PAST) version 1.38 (Hammer et al., 2001; Hammer and Harper, 2005). A paragenetic sequence for the Sinbad Limestone was also determined using these data.

Core plugs were taken from samples collected from the Spotted Wolf Panel using a drill press in the lab. Petrophysical measurements were completed using Brigham Young University's TerraTek Model 8400 nitrogen plug porosimeter-permeameter. Porosity-permeability cross plots were constructed from core plug petrophysical data and pore type was determined using nomenclature of Choquette and Pray (1970) and Lonoy (2006).

To develop a model that will enable us to predict fracture intensity (number of fractures per unit length of along a sample line) in the subsurface we collected data on spacing, width, orientation, and intensity of fractures in surface sections. Scan lines were chosen to represent contrasting sedimentary rock types and bed thicknesses. Calculation of fracture intensity was normalized using cumulative-frequency fracture size distributions described by Ortega et al. (2006).

MICROFACIES ANALYSIS

Microfacies are classified by lithology, frequency and composition of allochems, sedimentary structures, and texture. Abundance of allochems was determined qualitatively. The dominant allochem types are ooids, mollusk microbioclasts, mollusks that are compacted and contorted, whole mollusks, echinoderms, intraclasts, peloids, mud, and quartz silt. Microbioclasts represent finely comminuted bivalve debris. The

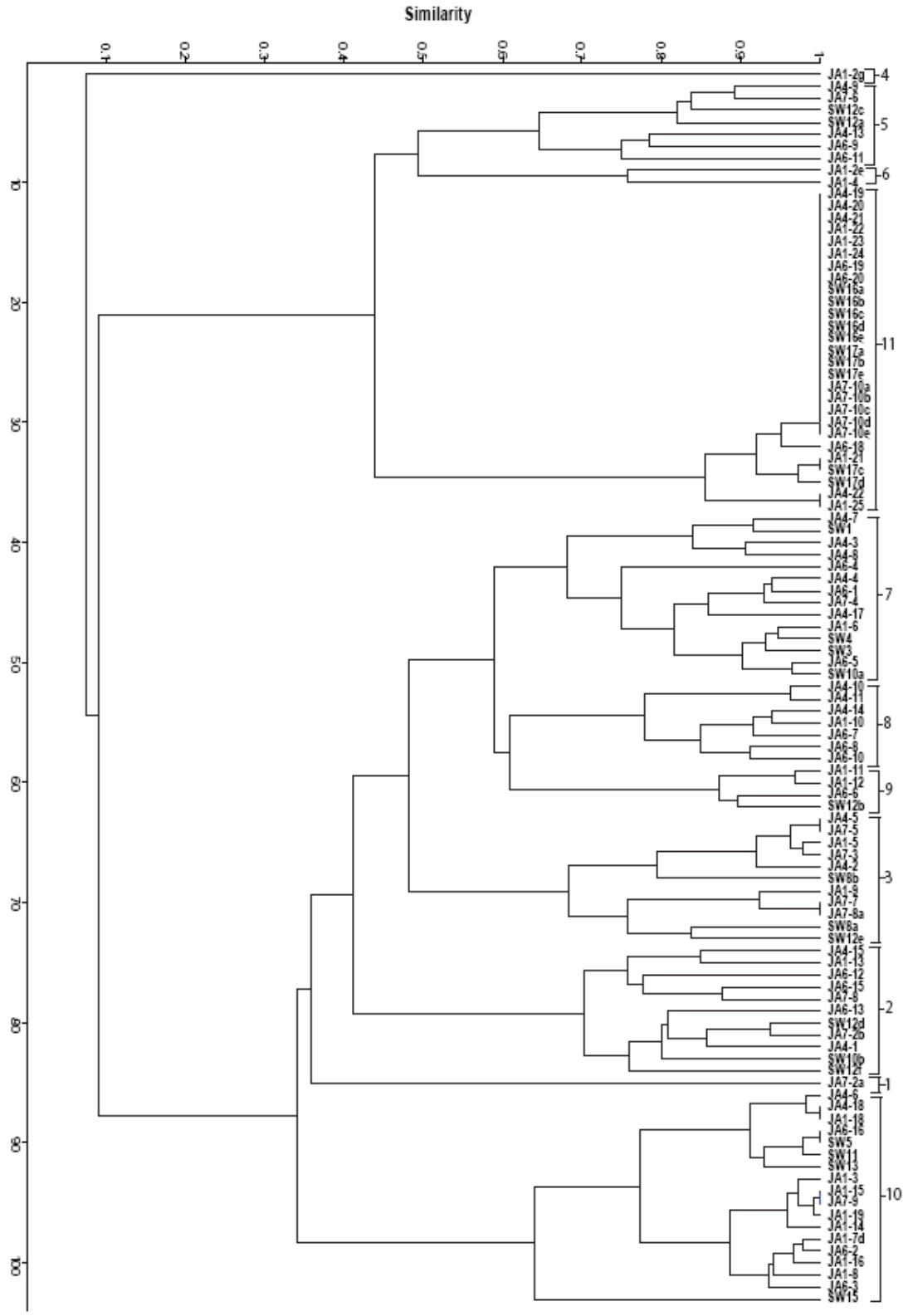

Figure 2. Cluster diagram of thin section abundances based upon Morista's index. Microfacies clusters are labeled 1-11.

dominant siliciclastic component is quartz silt; however, trace amounts of chert, feldspar, and muscovite are present.

Cluster analysis was conducted as prescribed by Ekdale et al. (1976). Grain abundances were coded from 0-4 following the procedure of Ehrenberg et al. (1998) with zero indicating that the allochem was not present, a score of one indicating less than two percent, two indicating a percentage ranging from 2-5, three representing percentages from five to 20%, and four indicating >20%. PAST (Hammer et al., 2001), a statistics package oriented towards paleontologists, was used for the clustering. Q-mode clustering using the unweighted pair-group average (UPGMA) algorithm was used on an 89 x 15 sample-by-attribute matrix. Samples were obtained from the samples collected from Sections 1, 4, 6, 7, and the Spotted Wolf section. Cluster analysis using Morisita's index for abundance data, an index that normalizes away absolute abundances, is insensitive to sample size (Hammer and Harper, 2006), and clusters samples together according to similarity, yielded 11 microfacies labeled one through eleven (Figure 2). Microfacies are numbered according to stratigraphic succession. Descriptions of microfacies follow below.

Microfacies 1—Stromatolite

Microfacies 11 is only found in Section 7-10, in the lowermost bed. This microfacies is very muddy (75%). Randomly distributed silt and void-filling spar are minor constituents. In outcrop, stromatolites are 150 cm long and 21 cm high (Fig. 3A, B). No algal structures or bedding are discernible within the stromatolite mounds (Fig. 3C). In the middle part of the mounds, breccia clasts are present.

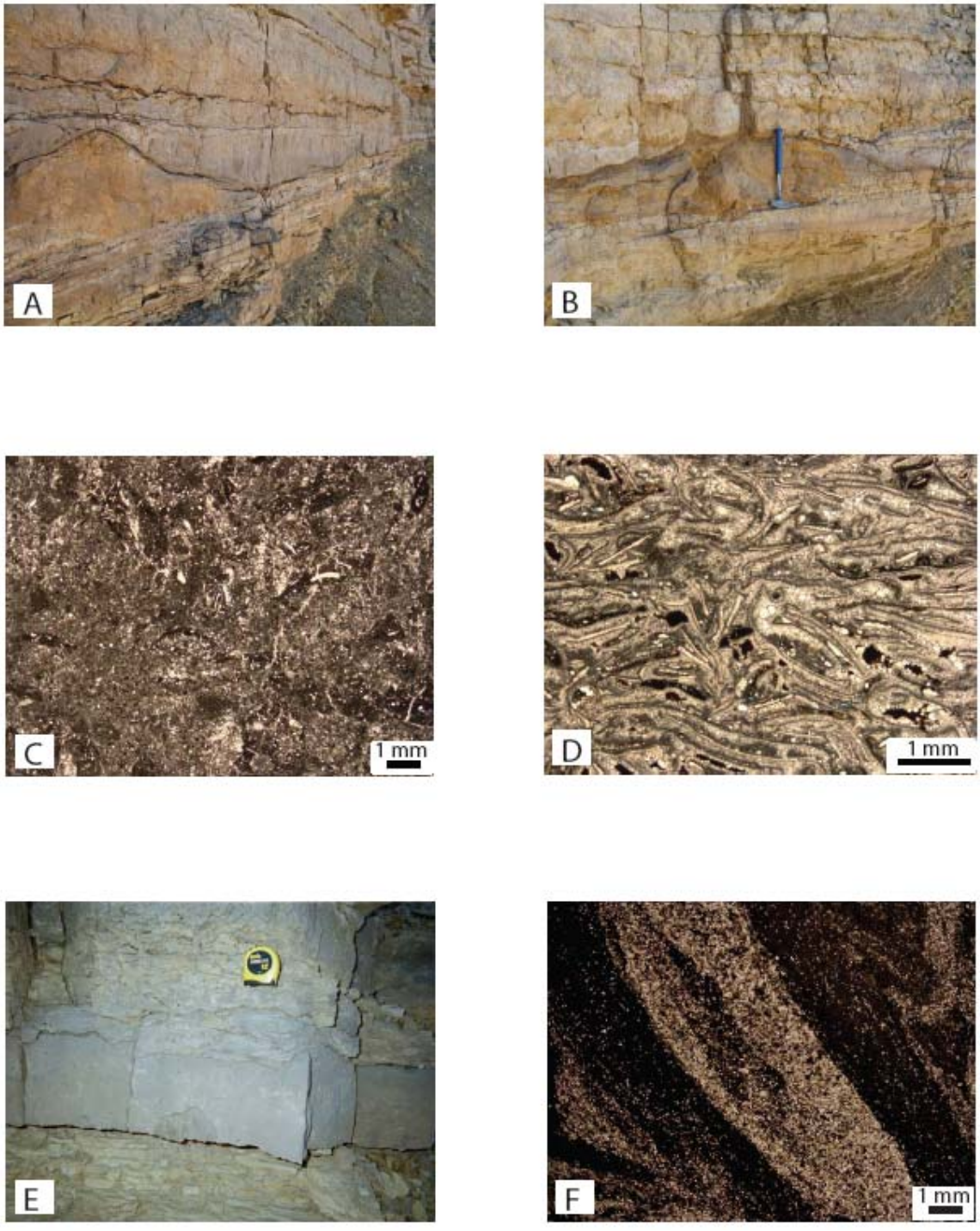

Figure 3. Selected photographs from Association A. A) Oblique view of stromatolite layer. Stromatolite is 21 cm high. B) Outcrop exposure of stromatolites. Hammer for scale. C) Chaotic nature of stromatolitic material of Microfacies 1. D) Deformed mollusks and perched mud of Microfacies 2. E) Outcrop of Microfacies 3 showing extensively bioturbated bed overlying and underlying a nonbioturbated bed. Tape measure for scale. F) Burrowed siltstone of Microfacies 8.

Microfacies 2—Overpacked Molluscan Grainstone

This microfacies is composed predominantly of grainstones and grain-dominated packstones of compacted and layered bivalve shells and gastropods. Mollusk shells are fragmented or articulated with disarticulated valves displaying compactional features (Fig. 3D). This facies has minor amounts of echinoderm fragments (0.5 X 0.25 mm), peloids—fine to very fine-grained, quartz silt, mud intraclasts, phosphatic material, minor quartz silt (1-5 mm long), and minor oxides. When present, mud is perched on bivalve shells. This facies is thin to medium bedded and is rippled.

Microfacies 3—Bioturbated Siltstone

This microfacies is very similar to Microfacies 11 except that all primary sedimentary structures have been obliterated by extensive burrowing (Fig. 3E, F). Because of the occurrence of limestone and siltstone in this microfacies, it is clustered between the limestone and siltstone microfacies.

Microfacies 4—Intraclastic Grainstone

This rare microfacies was found only near the basal portion of Section 1. Constituent intraclasts are subangular to subrounded and range from 0.25 mm to 3.5 mm (Fig. 4A). They are composed of a pinkish-yellow mud with minor amounts of quartz silt. This facies is interbedded with mudstones/siltstones that are ripple laminated and very thinly bedded.

Microfacies 5—Oolitic Molluscan Packstone/Grainstone

Ooids and mollusks are the dominant constituents of this microfacies (Fig. 4B, C). Ooid microfabrics are tangential and radial (Fig. 4D), ooids are medium to fine-grained, and have nuclei composed of mud. Complete to partial recrystallization of nuclei are

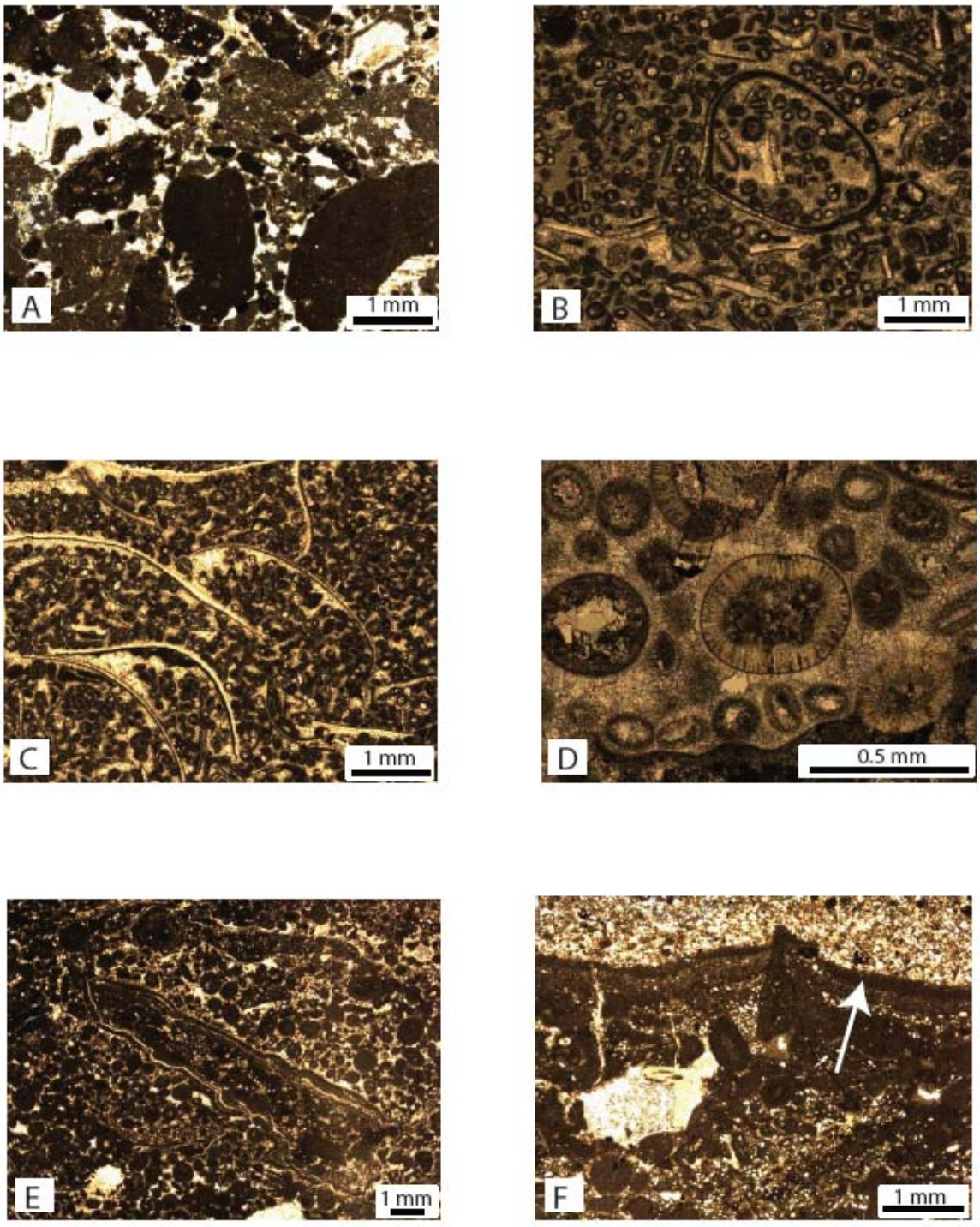

Figure 4. Selected photomicrographs from Association A. A) Intraclast-dominated sediment of Microfacies 4. B) Oolitic and mollusk rich sediment of Microfacies 5 showing a whole bivalve shell. C) Oolitic molluscan grainstone of Microfacies 5. D) Radial microstructure of ooids from Microfacies 5. E) Coated grains of Microfacies 6. F) Layering of Microfacies 3. Arrow points to mud-rich boundary between layers.

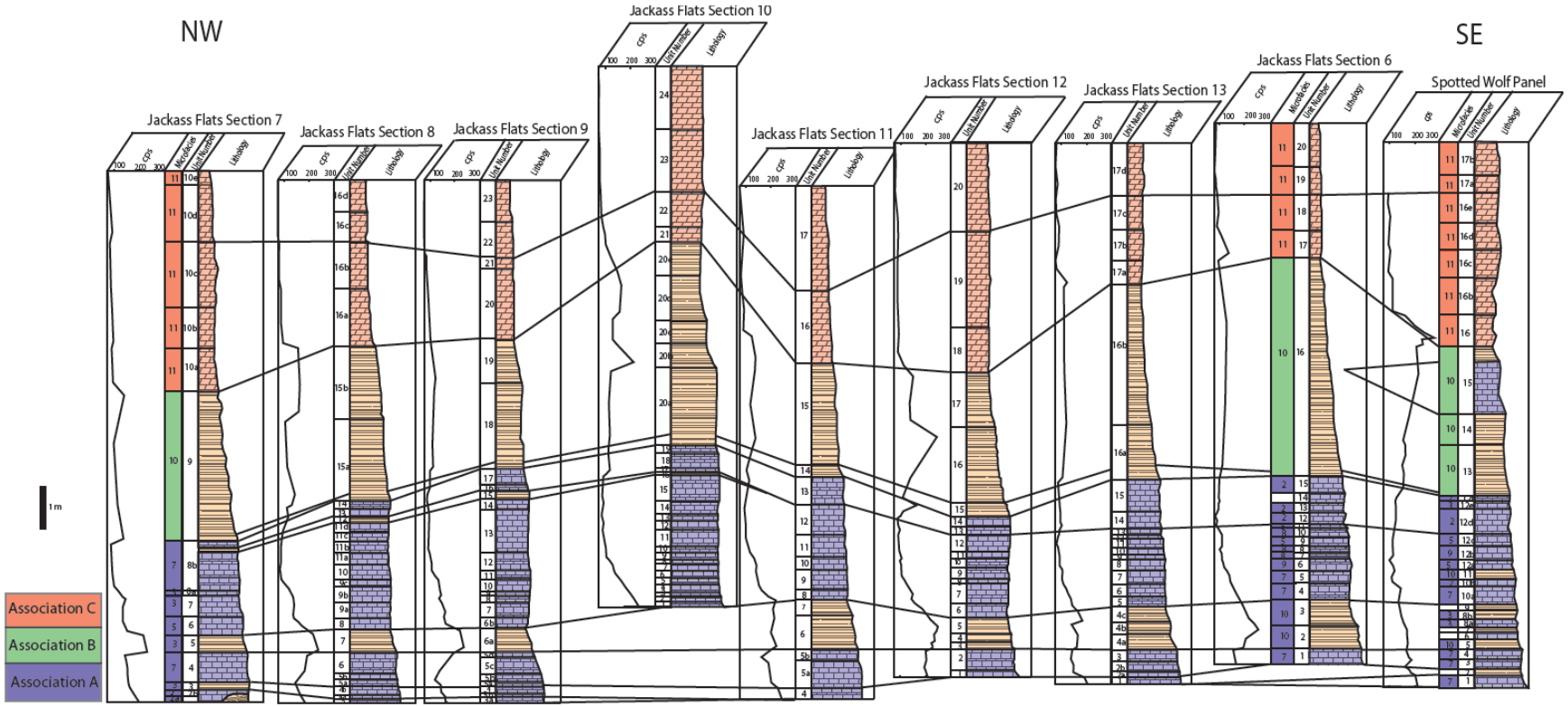

Figure 5. Diagram showing the correlation of beds measured within the Sinbad Limestone from the NW to the SE. For location of measured sections see Figure 1.

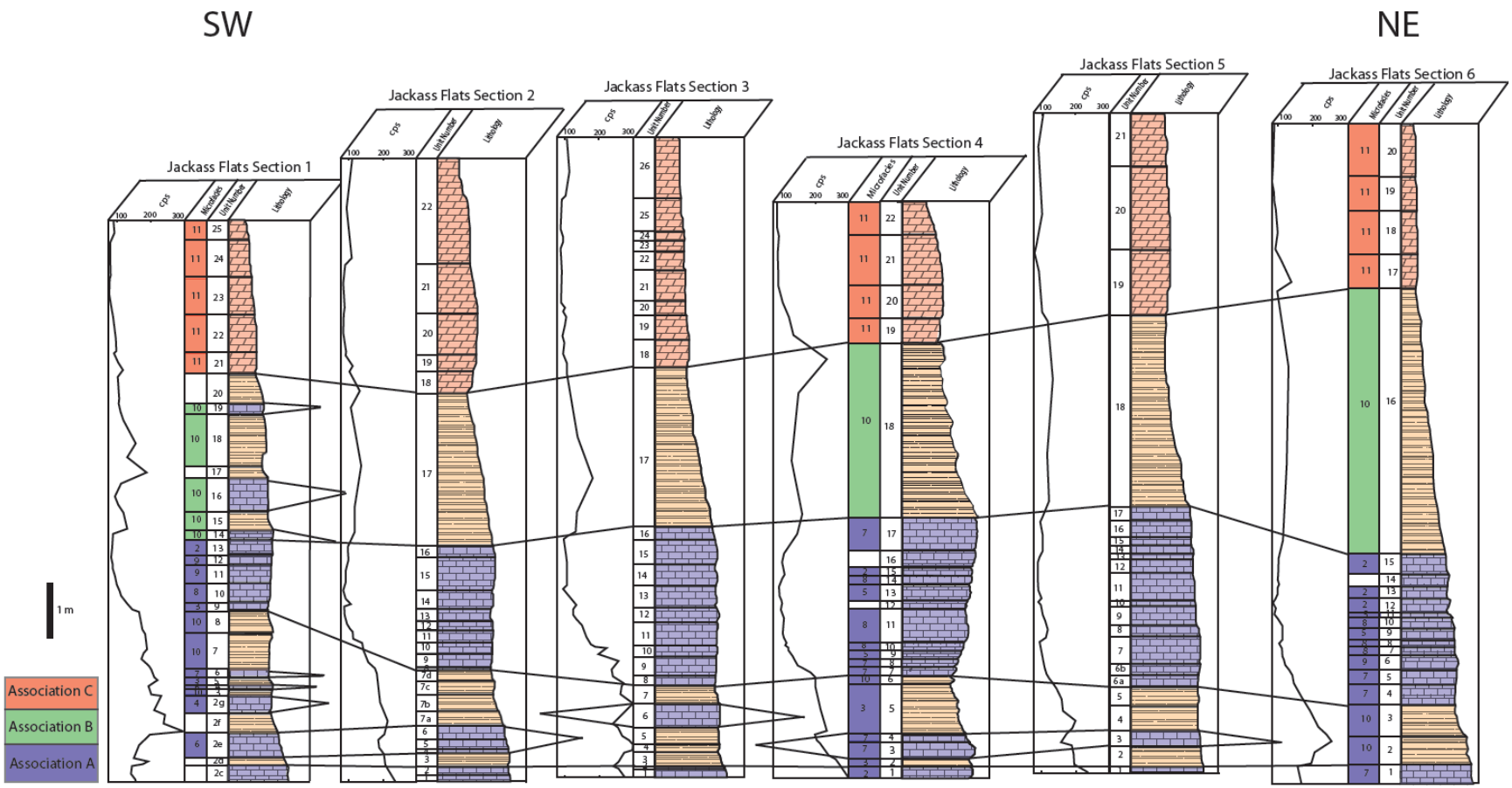

Figure 6. Diagram showing the correlation of beds measured within the Sinbad Limestone from the SW to the NE. For location of measured sections see Figure 1.

present in 10-30% of the ooids. Mollusks are articulated, disarticulated, or fragmented and comprise 5-20% of the rock. Mollusk fragments range from 0.5-2 mm but are commonly 1 mm in length. Gastropods (0.5-1 mm) or bivalves (1-5 mm) are the dominant biotic of this microfacies. Minor echinoderm fragments, very fine-grained peloids, and intraclasts (1-3 mm) are also present. All beds have abrupt upper contacts. Ripple lamination is evident on outcrop.

Microfacies 6—Coated-Grain Grain-Dominated Packstone

This microfacies was found within only two samples in Section 1, JA1-2e and JA1-4 (see Figures 5, 6). Coated intraclasts are the dominant constituent of the lowermost sample. These allochems (oncoids?) lack biotic microstructure (Fig. 4E). Tangential ooids comprise 5-15% of the rock. Most are 0.5-1 mm; however, a few are ~2 mm in diameter. Coated intraclasts range from 1.5-9 mm in length; uncoated intraclasts are also present. Silt increases in abundance towards the top of the bed. Within the thin section, there are four layers. The lowest layer is comprised of closely packed ooids, intraclasts, and mud followed by a layer of coated intraclasts and loosely packed ooids. The third layer shows a decrease in coated grains with an increase in silt which is overlain by a layer of pure silt (Fig. 4F). Dividing these areas are layers of laminated mud. The second thin section does not have any dividing layers, or silt. The predominant composition is coated grains and intraclasts.

Microfacies 7—Molluscan Peloidal Grain-Dominated Packstone

In this microfacies (Fig. 7A), gastropods and bivalves are abundant and some microbioclasts and whole shells are present. Gastropods range from 2-4 mm in length. Bivalves range from to 1-8 mm in length. Microbioclasts are comprised of broken bivalve

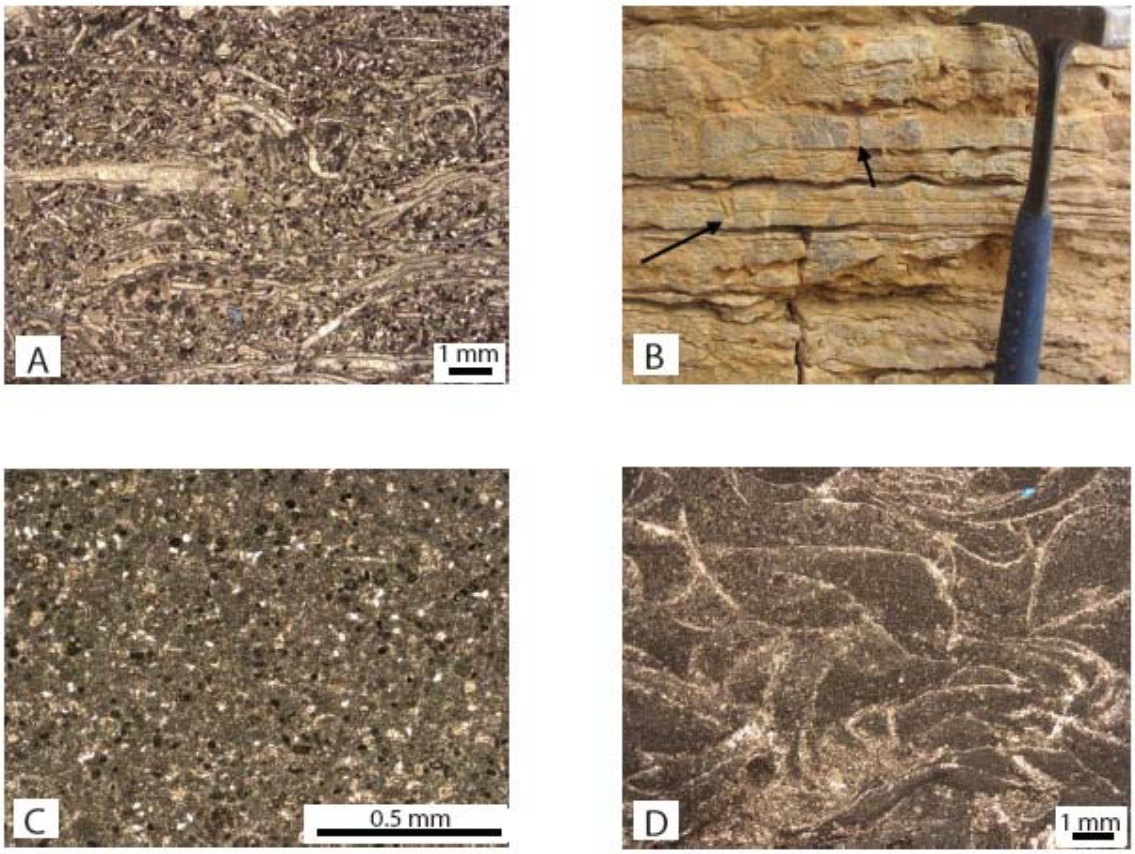

Figure 7. Selected photographs of Association A. A) Microbioclast-rich sediment of Microfacies 7. B) Outcrop of Microfacies 5 showing *Skolithos* burrows (arrows). Hammer for scale. C) Peloid-rich sediment of Microfacies 6. D) Thin-shelled bivalves of Whole-Fossil Wackestone of Microfacies 7.

shells and echinoderm fragments. Crinoid columnals and echinoderm spines are both common. Mud is also common. Minor fine-grained peloids, well-rounded, yellow, silty intraclasts (average 3.5 mm X 1 mm), oxides, and quartz silt are present. Bioturbation and *Skolithos* burrows (Fig. 7B) are common. Ripple lamination is also present in some areas.

Microfacies 8—Peloidal Grain-Dominated Packstone/Grainstone

This facies is characterized by the large percentage of fine-grained peloids (Fig. 7C). Microbioclastic and whole bivalves locally make up ~10% of the rock. Whole bivalves average 2.5 mm long and microbioclasts are commonly <1 mm long. Minor

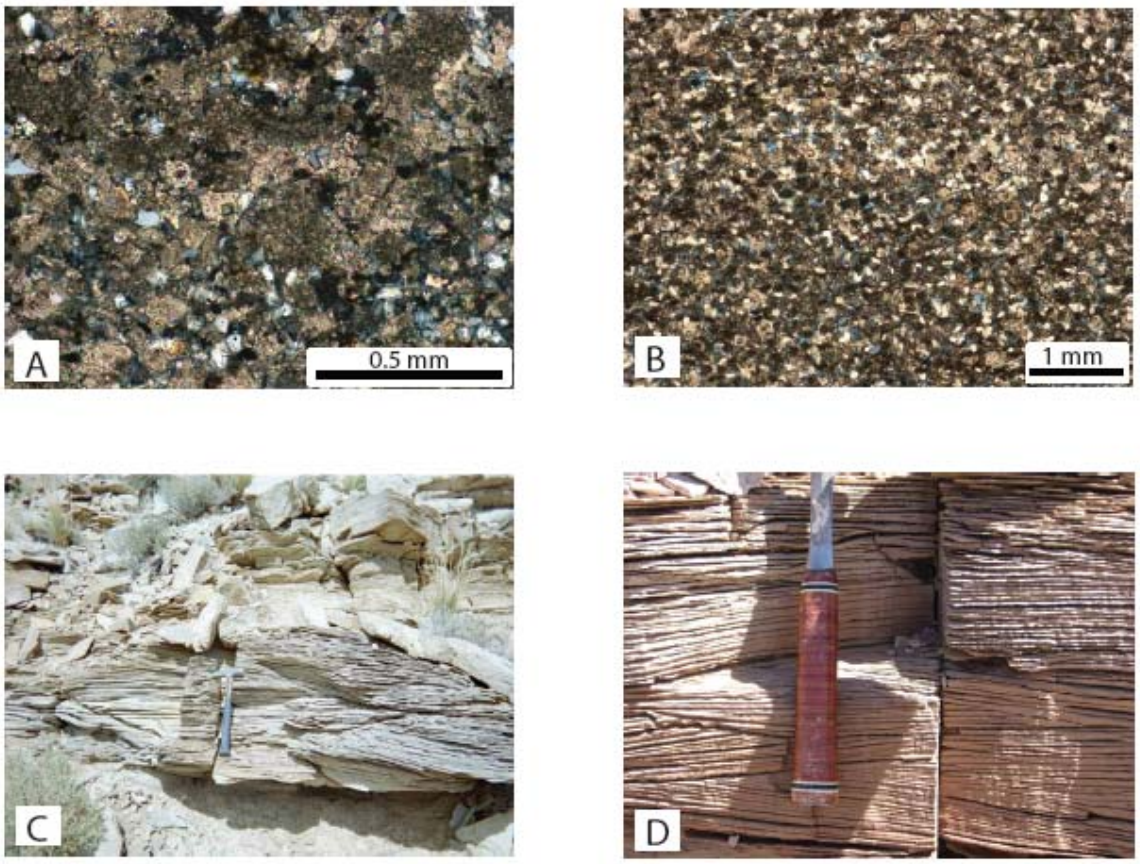

Figure 8. Selected photographs of Association B. A) Photomicrograph of silt-rich end-member of Microfacies 10. B) Peloid-rich sediment of Microfacies 10. C) Outcrop of hummocky cross-stratification. Hammer for scale. D) Outcrop of Association B showing hummocks and platey weathering. Hammer for scale.

amounts of echinoderms, brown muddy intraclasts (average 1.5 mm X 1 mm), quartz silt, and mud are also present. Planar lamination and rippled bedding planes are very common.

Microfacies 9—Whole-Fossil Wackestone

Mud makes up more than half of this facies with minor amounts of whole bivalveshells, peloids, silty intraclasts that average 4.5 mm X 2.5 mm, and silt (Fig. 7D). Bivalve shells are thin and can reach up to 6 mm in length.

Microfacies 10—Laminated Silty Peloidal Grainstone to Peloidal Siltstone

Microfacies 3 is composed of siltstone (Fig. 8A) and peloidal grainstones

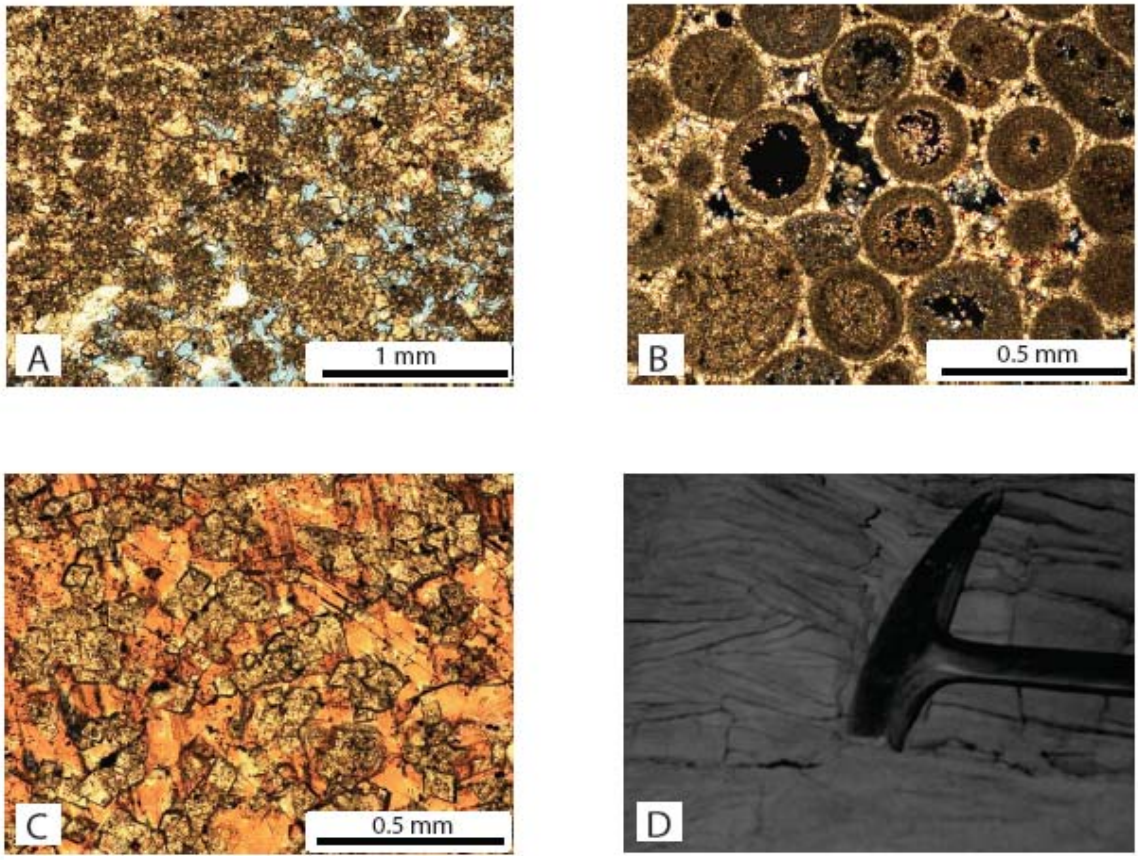

Figure 9. Selected photographs from Association C. A) Dolomitized ooids of Microfacies 11. B) Ooids from Microfacies 11 that have not undergone Dolomitization. C) Dolomite rhombs from Microfacies 11. Outcrop of Association C showing herringbone cross-beds. Hammerhead for scale.

(Fig. 8B). Laminae are visible in thin section. The relative dominance of silt and peloids has led to two end-members of this microfacies. These members are grouped together into this microfacies because of diagnostic sedimentary structures. In the silt-rich end-member peloids are present, but are not as common. Mud comprises less than 5% of the rock. The peloidal grainstone end-member is composed of fine-grained, recrystallized peloids. Minor amounts of echinoderms and silty-mud intraclasts (2.5 mm diameter) make up a few percent of this rock. Planar bedding, scour and fill, trough cross-stratification, and horizontal trace fossils are common within this facies. Hummocky cross-stratification (HCS) (Fig. 8C) is also present in the middle portions of all measured sections and weathers into plate-like sheets (Fig. 8D).

Microfacies 11—Oolitic Grainstone

This microfacies, composed of ooids comprise the upper member of the Sinbad in the study area. Bivalves are rare, with 5% present locally. Regionally, the ooids are dolomitized (Fig. 9A) except for two samples from Section 1 and 4 (Fig. 9B). Ooids are fine-grained and apparently underwent extensive micritization, prior to becoming dolomitized. Dolomitized ooids (individual rhombs are 30 microns) are finely crystalline and are cemented by calcite and dolomite (Fig. 9C). The degree of dolomitization varies from sample to sample. In some samples, there are traces of cortical fabric (the part of an ooid surrounding the nucleus); in others dolomitization was fabric destructive and precursor oolitic composition is assumed. Trough cross-stratification, planar lamination and herringbone cross-beds (Fig. 9D) are present in outcrop.

Interpretation of Microfacies Patterns

In the area of the San Rafael Swell, the Sinbad Limestone is composed of three distinct facies associations (Fig. 5, 6). The lowermost association (A) is composed predominantly of limestone, representing two cycles of deposition on a shallow storm-dominated ramp. The middle association (B) is composed of peloidal siltstones, and the upper association (C) is composed of dolomitized oolitic grainstones.

The Sinbad Limestone is underlain by peritidal siltstones of the Black Dragon Member of the Moenkopi Formation (Blakey 1973b). The contact is a scoured surface with 3-5 cm of erosional relief. In measured sections 7-10 (Fig. 5), this surface is overlain by low, domal stromatolites of Microfacies 1 with 20 cm of constructional relief. Water depths were very shallow and are intertidal/shallow subtidal (Logan et al., 1964). This relief is filled by a storm-deposited bed of Microfacies 2 or in other localities

Microfacies 4 or 5 (Fig. 6, 10A). Perched mud within Microfacies 2 and intraclastic grainstones of Microfacies 5 indicate deposition by storms (Tucker and Wright, 1990). Stromatolite beds thin to the west and eventually pinch out completely. An encrusted hardground (Fig. 10B, C) marks the top of the relief-filling packstone. The hardground is developed within storm-deposited sediments, and can be traced through all measured sections. Overlying sediments associated with the hardground are bioturbated silty peloidal limestones of Microfacies 3. These show evidence of scouring and an increase in silt to the east and reflect burrowing of organisms into storm-deposited sediments. Graded bedding, an intraclast-rich base and bioturbation characterize the next bed. This package of sediment is easily traceable throughout the studied area (Fig 5, 6).

Above this bed, the dominant lithology is siltstone (Fig. 10D). Within this unit there are three beds, the first and last which are mechanically deposited, and the middle bed which is extensively bioturbated. Burrows are also present at the top of the upper bed. This clastic unit is present throughout the entire area. In sections that are further west, i.e. Sections 1-5, interbeds of limestone are present that pinch very rapidly (Fig. 10E). Because of the silty nature of this unit, it has been interpreted as aeolian fallout on the exposed Sinbad shelf after regression of the ocean. As the sea transgressed back over the shelf, these deposits were reworked and spread over the entire area. Interbeds of limestone represent carbonate material washed landward by storms. Transgression continued up to a depth above storm wave base but below fair weather wave base ending deposition in this parasequence.

After deposition of the siliciclastic material, a new parasequence developed with continuation of carbonate sedimentation (Association A). Upper limestones of

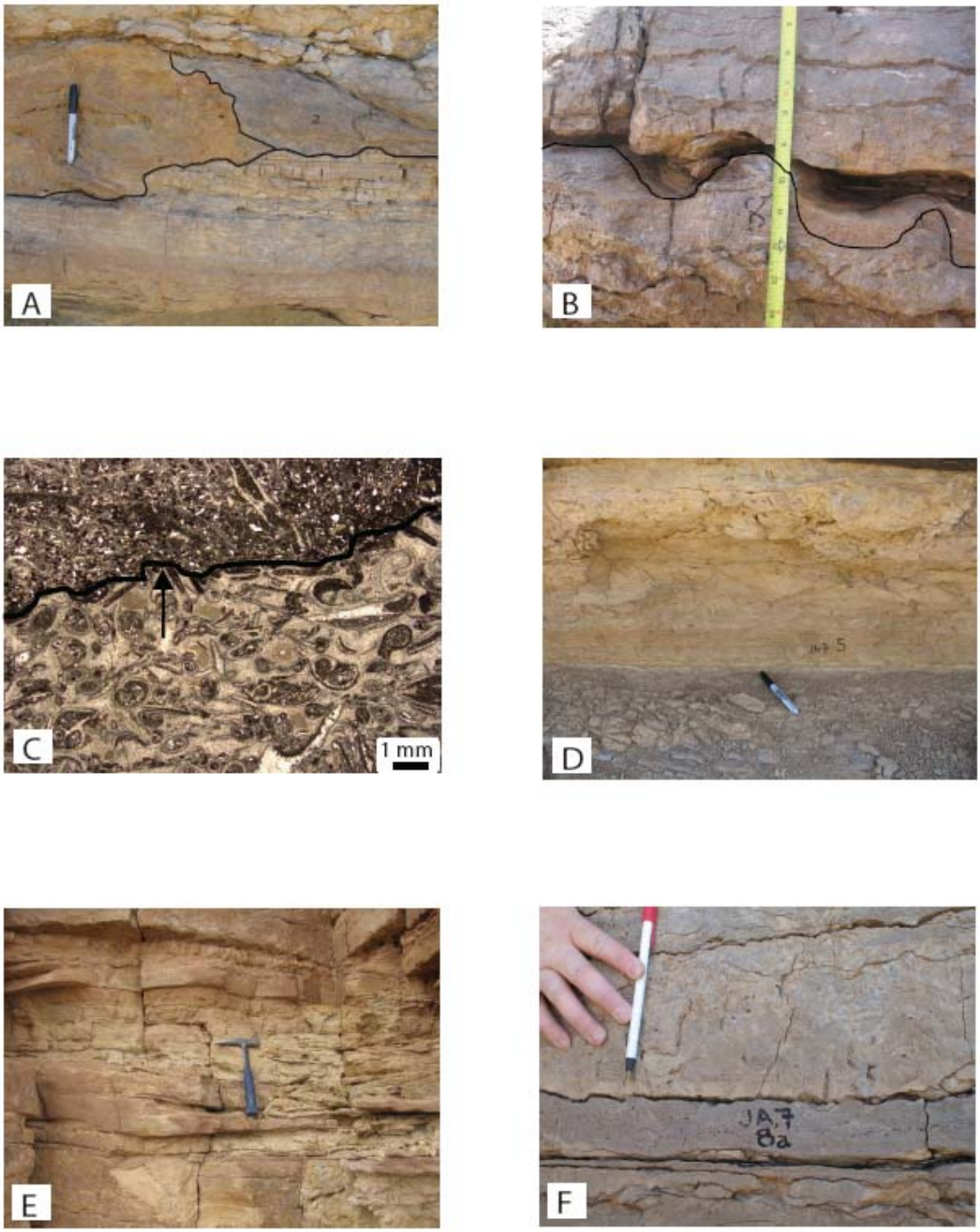

Figure 10. Selected photographs from the Sinbad Limestone. A) Outcrop of stromatolitic material that shows a scoured top and base as well as infilling of accommodation space by sediment of Microfacies 2. B) Outcrop of hardground surface. Tape measure for scale. C) Photomicrograph of hardground surface with truncated grains (arrow). D) Transgressive siltstone near the base of the Sinbad Limestone. Marker for scale. E) Photograph showing pinching out of limestone beds (reddish-brown) in transgressive silt (orange-brown). F) Mechanically-deposited bed under and overlain by bioturbated beds.

Association A are characterized by beds of mechanically deposited and bioturbated sediments (Fig. 10F). Mechanically deposited sediments contain a wide variety of structures including hummocky and trough cross-stratification, planar lamination and ripples. Overlying each storm-influenced package are bioturbated, homogenized packages. These bioturbated beds reflect time between storms when the energy level was low enough for infauna to resume burrowing and churning the sediment. As many as four cycles of mechanically-deposited and bioturbated packages are present. Beds within this facies do not extend throughout the entire area except for one siltstone bed and the uppermost cycle which thickens along strike (Fig. 5). Individual beds pinch and swell and are difficult to correlate; however, the general pattern is present throughout the entire area (Fig. 5, 6). Sections further west contain more hardgrounds, (up to three), and more siltstone interbeds. Hummocks indicate that this sediment was deposited by storms (Dott and Bourgeois, 1982). Goodspeed and Elrick (1993) conclude that this association comprised a transgressive systems tract. Capping the limestone association is a bed of shale which is regarded as the maximum flooding surface within the Sinbad Limestone (Fig 5, 6).

Association B constitutes a major portion of the Sinbad Limestone (Fig. 5, 6). Based upon predominance of storm-generated sedimentary structures, water depth, appears to be very similar to water depths of Association A. However, where the lower unit has a diverse fauna, the middle unit is dominated by silt and peloids. There are two possible explanations for this major lithology shift. The first possibility is a major influx of terrigenous sediment from a proximal highland which killed the organisms in the area and shut down the carbonate factory. The closest highland during this time was the

waning Uncompaghre uplift (Blakey, 1974) and is unlikely to have provided this sediment. Many of these sediments are peloid grainstones that cannot have come from this uplift. The other explanation is a restriction of water further out on the ramp. The restriction caused a decrease in the carbonate factory and the formation of peloids. Water restriction is attributed to either an oolitic shoal or reef. As this Thaynes-equivalent barrier grew, it decreased water circulation and caused a major shift in lithology of the inner shelf.

Above Association B, relative water depth decreased and oolites of Association C were deposited (Fig. 8, 9). Herringbone cross-beds, prograding ooid-rich packages, and oolitic sediments of Microfacies 11 are strongly suggestive of tidally-influenced ooid shoals (Tucker and Wright, 1990).This association represents the development of ooid shoals and tidal channels. This package of sediment reflects highstand (Lutz, 1993;

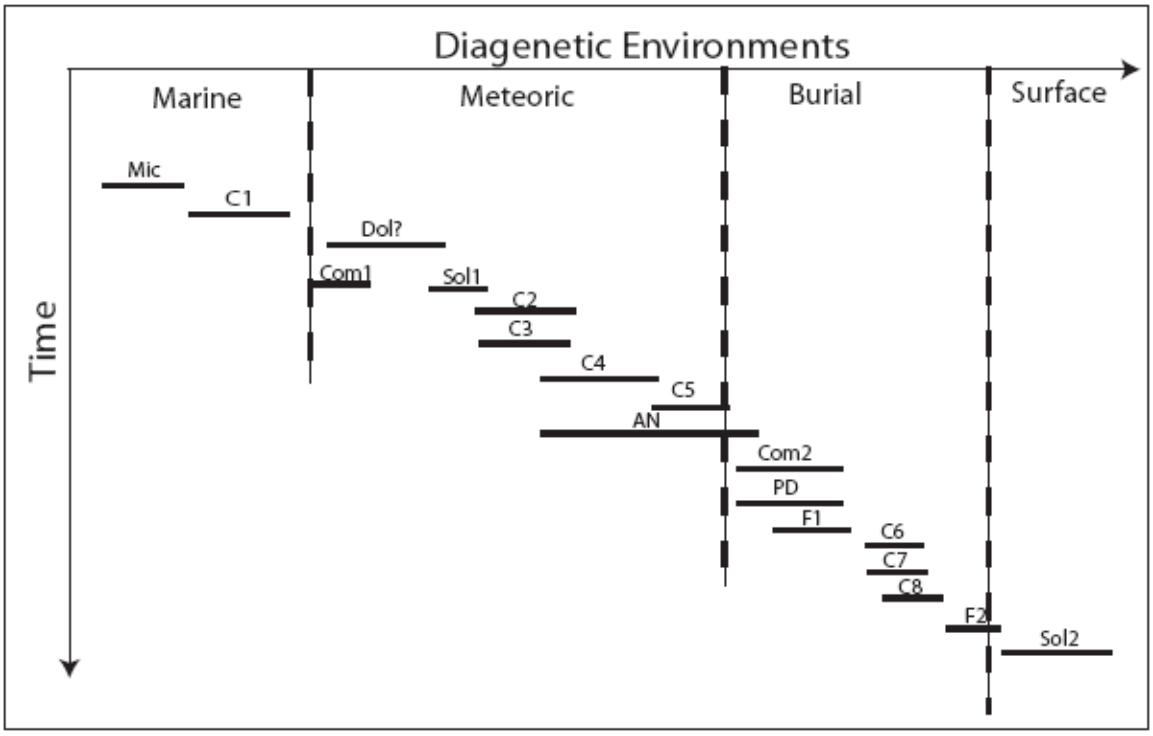

Figure 11. Paragenetic sequence inferred for Sinbad diagenetic features.

Goodspeed and Elrick, 1993) to falling stage conditions as evidenced by the low relative sea level and progradation of ooid shoals basinward. After deposition of this association, carbonate deposition ceased and deposition of basal siltstones and mudstones of the Torrey Member commenced.

DIAGENETIC FEATURES

Diagenesis within the Sinbad Limestone is ubiquitous. Diagenetic features are often related to the presence/absence of mud, original chemistry of the particle, and the texture of the rock. Diagenesis appears to be strongly controlled by microfacies association. Limestones of Association A typically show micritization, fibrous isopachous cements, neomorphism of molluscan grains, equant and drusy spar, and fracturing. Association B shows euhedral dolomite rhombs, silica and calcite cementation, pressure solution, and fracturing. Ooids of Association C are micritized, dolomitized, and compacted. They are also cemented by poikilotopic calcite cement. The paragenetic sequence is shown on Figure 11. Listed below are common diagenetic features and an interpretation of the environmental setting in which they formed.

Micritization

Many fossils have a thin micrite rim (about 20 microns thick); however many ooids have been completely micritized leaving only traces of original cortical structure (Fig. 12A). Micritized carbonate grains are common throughout the study area except for mud-rich and silt-rich rocks of Microfacies 6, 7 8, 10, and 11. Micritization is caused by endolithic algae and as such occurred in the shallow marine environment within the photic zone (Tucker and Wright, 1990).

Fibrous Isopachous Cement

Fibrous isopachous cement needles average 50 microns long and less than 10 microns wide with sharp, pointed terminations (Fig. 12B). This type of cement is found in Microfacies 2, 5, and 9. This cementation is indicative of marine phreatic environments (Heckel, 1983). In the Sinbad Limestone, it is also commonly associated with hardgrounds (Fig. 12C).

Dolomitization

Dolomitization is constrained to two microfacies: the oolitic grainstone, and siltstones of Microfacies 10. Dolomite descriptions follow that of Tucker and Wright (1990). Dolomite rhombs are planar e to planar s, mimetic to nonmimetic, and range from medium to very finely crystalline varieties (Fig. 12D). Typically the medium and fine varieties are planar-euhedral, while the very finely crystalline varieties are planar-subhedral. In one sample from the Spotted Wolf panel, the dolomite crystals are nonmimetic, non-planar and very coarsely crystalline. Zoned subhedral to euhedral dolomite crystals (80 microns) as found in Microfacies 10 (Fig. 12E) grew displacively within the calcite cement. Planar e and planar s crystal types are interpreted to have formed under low temperature conditions (Tucker and Wright, 1990) suggesting that dolomitization in this area occurred early.

Dolomitization as discussed above formed in low temperature environments. Due to the landward position of the dolostones, the early, shallow subsurface origin of dolomitization, the absence of evaporites, and the highly porous nature of the protolith, dolomitization is interpreted to be the result of the mixing of freshwater and seawater (Tucker and Wright, 1990). Geochemical work is necessary to provide further evidence

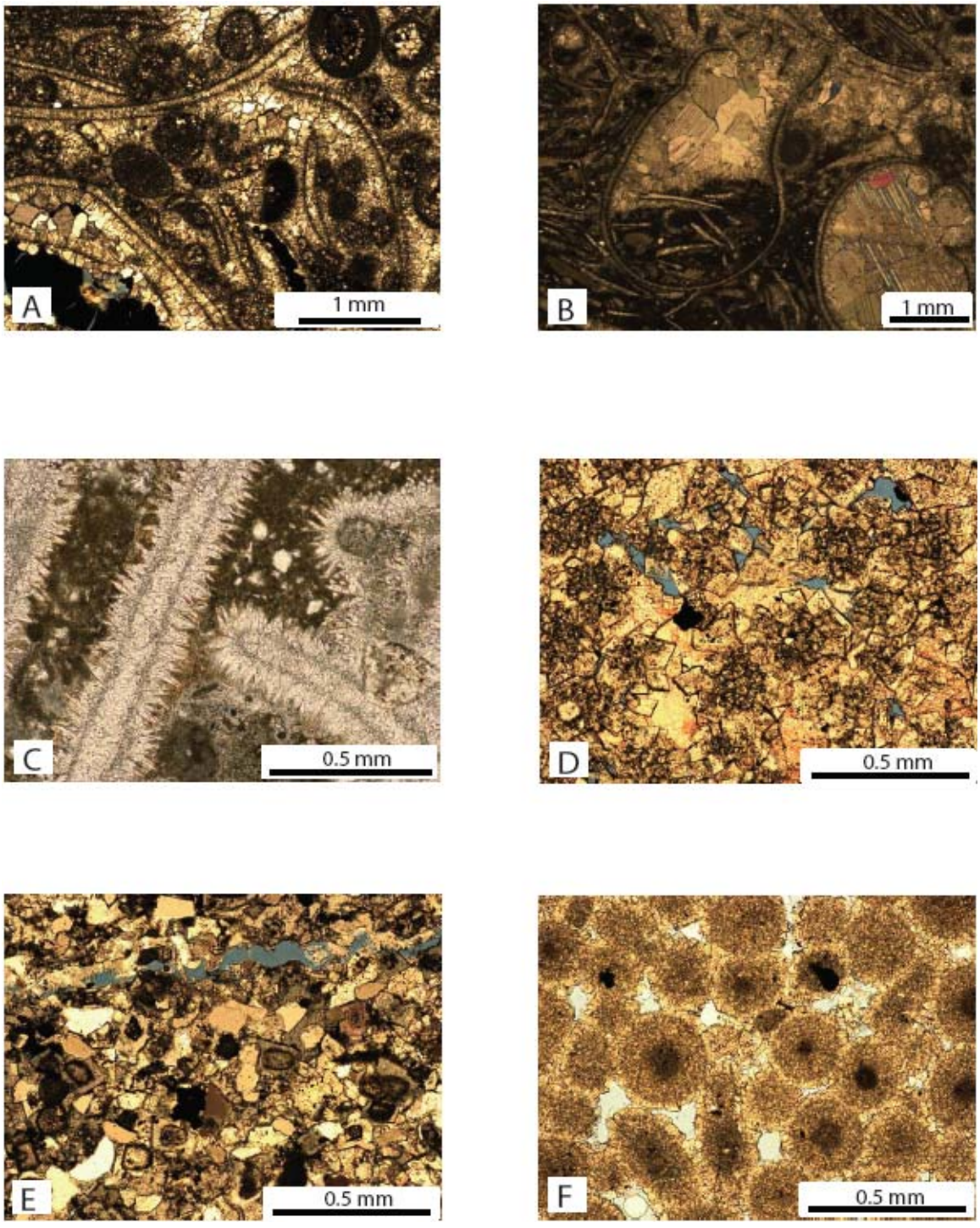

Figure 12. Photomicrographs of selected diagenetic features. A) Micritized grains, fibrous cements, and recrystallized oil of Microfacies 5. B) Isopachous fibrous cement, and infilling sediment and spar within a gastropod shell. C) Isopachous fibrous cement found associated with hardground. D) Planar e dolomite rhombs of Microfacies 11. E) Zoned dolomite rhombs that have grown displacively in calcite cement from Microfacies 10. F) Preserved oolitic microstructure of undolomitized ooids.

of the dolomitization model. Several samples within the dolomite section were not dolomitized, all of which are located at the top of the measured sections (Fig. 12F). Dolomitization possibly did not occur because of the position of these packages of rock closer to the surface. Because of their location, sufficient temperatures and mixing of fluids did not occur and they remained unaltered.

Dissolution

Most of the mollusks have undergone dissolution and reprecipitation of cement in the voids. All microfacies with mollusk shells have undergone this type of diagenesis. This occurred in the meteoric diagenetic environment where the water is saturated with respect to calcite but not to aragonite. In Microfacies 1, 3, 4, and 11, poikilotopic calcite cleavage plane dissolution (Fig. 13A) has taken place probably associated with exposure of the rocks to meteoric water during uplift.

Neomorphism

It is rare to find molluscan grains that have undergone replacement or recrystallization. A few cases (Fig. 13B, C), however, are present in Microfacies 5, 6, 7, and 9. Some originally calcite shells still retain the original prismatic fabric, while in others the aragonite has been completely replaced. These shells are composed of coarse prisms that extend from one shell wall to the other and probably indicate a complete removal of a secondary, aragonite shell layer (Scholle and Ulmer-Scholle, 2003). Aggrading neomorphism of micrite is abundant within muddy sediments as well. Neomorphism typically occurs in the meteoric diagenetic environment under slow-moving waters that are supersaturated with $CaCO_3$ (Heckel, 1983).

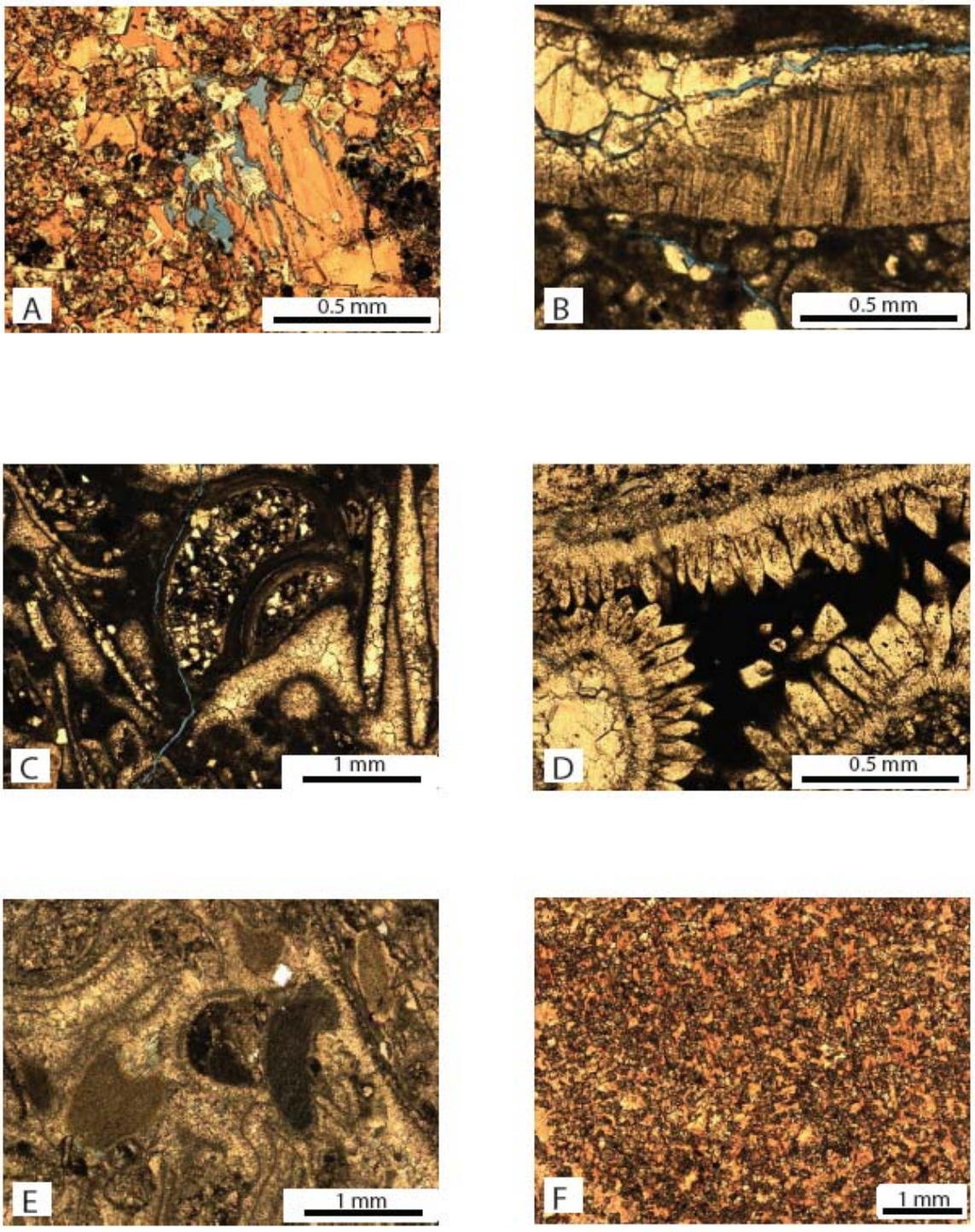

Figure 13. Selected photomicrographs of diagenetic features. A) Dissolution along calcite cleavage plane. B) Advancing front of dissolution and reprecipitation of calcite cement. C) Gastropod shell with preserved microstructure. D) Photomicrograph showing two generations of isopachous fibrous and bladed cement. Interparticle porosity filled with dehydrated oil. E) Syntaxial cement that has grown onto echinoderm fragments. F) Poikilotopic calcite cement grown around dolomitized ooids.

Equant and Bladed Isopachous Cement

Equant isopachous cement is fine to very finely crystalline and has euhedral crystal terminations. Crystals average 50 microns in size. This cement is present in Microfacies 1, 3, and 5. Commonly associated with the equant isopachous cement is a bladed isopachous cement. This cement averages 120-60 microns long and 60-20 microns wide (Fig. 13D). This cement is also found in Microfacies 1, 3, and 5. These cements were deposited under meteoric phreatic conditions (Scholle and Ulmer-Scholle, 2003).

Syntaxial Overgrowths

Syntaxial overgrowths occur on mud-poor rocks which also contain echinoderm fragments. Overgrowths are clear and free of dolomite inclusions (Fig. 13E). This cement is very small and is commonly less than 5% of the rock. Because of the clear and inclusion-free nature of the syntaxial cement, the cement is probably precipitated in a meteoric phreatic environment (Folk, 1974).

Equant Spar

Major porosity-reducing cements are equant calcite spar in nature. These cements are present throughout all thin sections and microfacies. This cement is clear with planar intercrystalline boundaries. Equant pore-filling cement is also a product of the meteoric phreatic environment (Scholle and Ulmer-Scholle, 2003).

Drusy Spar

Drusy spar is commonly associated with the equant pore-filling cement. Drusy spar is crystals of calcite that increase in size towards the center of the pore. Like equant

spar, this is another cement that reduces or completely fills pore space. It is also clear with planar intercrystalline boundaries. A drusy mosaic is believed to form in the burial environment (Scholle and Ulmer-Scholle, 2003). This cement is pervasive throughout all microfacies.

Poikilotopic Cement

Poikilotopic cement (Fig. 13F) is calcite cement that is larger than several grains of sediment together. This cement is clear with planar crystal boundaries. This type of cement is found in Microfacies 1, 3, 4, 8, and 11. This cementation is also the type that is most responsible for reducing intercrystalline porosity of many of the dolostones to <1%. This cement precipitates in the burial environment (Heckel, 1983).

Silica Cement

Silica cement occurs in two forms: quartz overgrowths, and fracture filling. Fracture-filling silica cement is light gray in color and is only found within Microfacies 1, 3, and 9. Quartz overgrowths are rare and only discernible by faint lines of fine-grained material separating the cement from the grain. They are only found in Microfacies 8 and 11. It is unknown whether the fracture-filling cement or the formation of quartz overgrowths formed congruently or not. Silica cement is a cementation event that occurs with deep (~100-2000 m) burial (McBride, 1989).

Compaction

Compaction is locally abundant and is common in oolitic-rich and bivalve-rich microfacies. In Microfacies 2, many of the bivalve shells have been compacted and contorted (Fig. 3D). In Microfacies 5, many of the ooids have undergone plastic deformation and brittle fracture and spalling of the ooid cortex (Fig. 14A). This process

is considered to be indicative of the burial diagenetic environment (Heckel, 1983); however, the early compaction of Microfacies 2 is a surface phenomenon due to loading and overpacking of the sediment before it shows modifications indicative of the meteoric environment.

Pressure Solution

Stylolites (Fig. 14B) and dissolution seams are the two types of pressure solution that occur within the Sinbad Limestone. They do not appear to be microfacies-controlled and can be found in multiple microfacies and lithology types. Stylolite description follows that of Railsback (1993). Stylolites have a thickness of 10-50 microns, amplitude of 150-500 microns, irregular surface of 50-110 microns and a frequency of three per 1000 microns. These are characteristic of the burial diagenetic environment.

Fracturing

Evidence of two episodes of fracturing occurs within the Sinbad Limestone. The earlier fracturing event is often filled by either silica or calcite cements (Fig. 14C) and does little to generate porosity. This cement-filled fracturing event formed in the burial environment. Most porosity is the result of a late stage fracturing event. It is unknown whether this event was due to burial or the unroofing of the sediment.

Dehydrated Oil

Dehydrated oil (Fig. 14D) is most common in Microfacies 2 and 11. Of ten thin sections of Microfacies 9, eight contain dehydrated oil. Much of this oil is found in interparticle and fracture porosity. Many vugs within the dolostones caprock are filled by the oil. It is unknown when the oil migrated through this region.

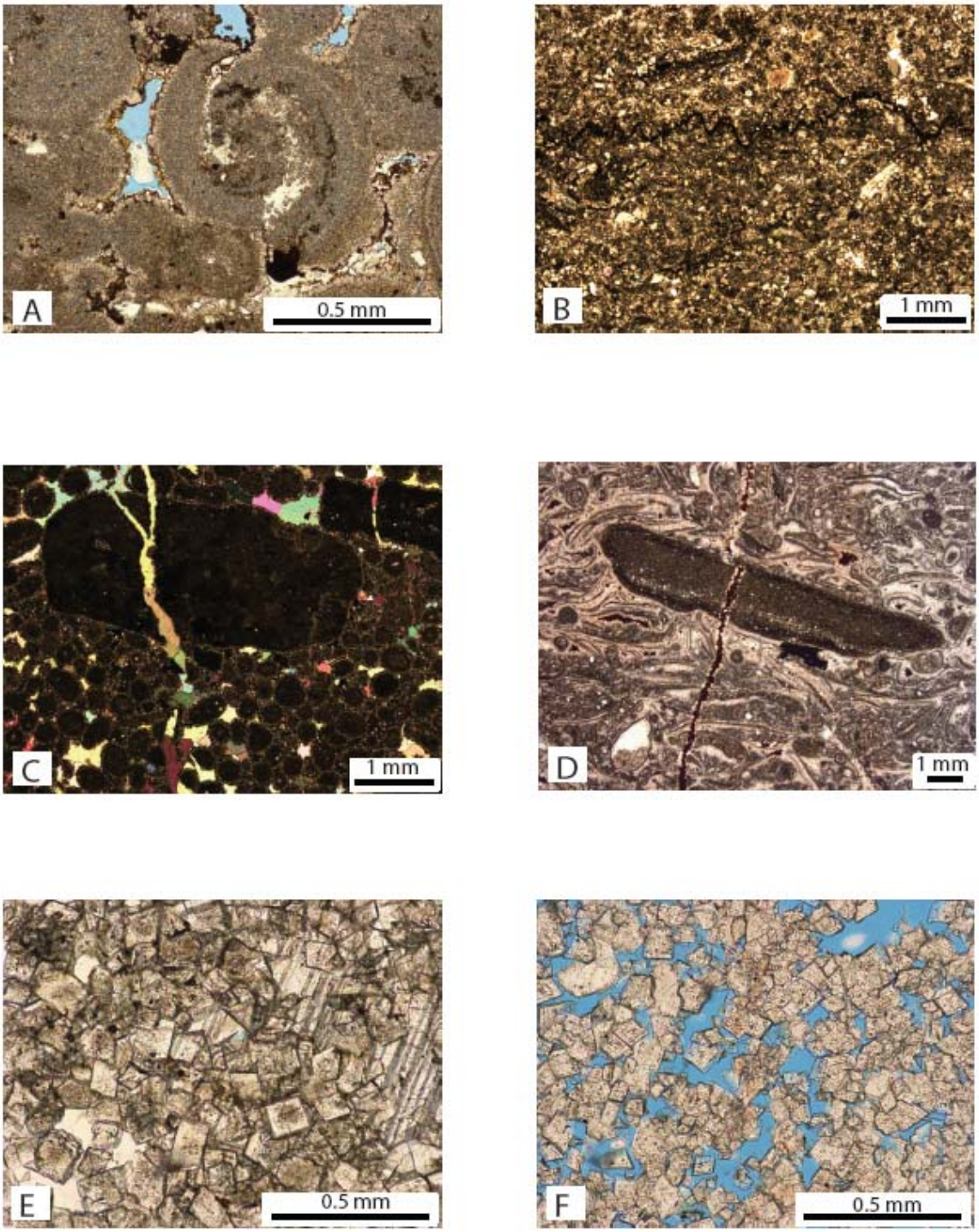

Figure 14. Selected photomicrographs of the Sinbad Limestone. A) Compaction of an ooid which has resulted in it breaking in half. B) Stylolite filled by oxide-rich material. C) An early cement-filled fracture from the first fracture event. D) An oil-filled fracture from the second fracture event. E) Dolostone displaying little to no porosity and infilling calcite cement. F) Dolostone showing high porosity and no remnants of calcite cement.

RESERVOIR CHARACTERIZATION

Thin Section Porosity

Thin section porosity is grouped according to microfacies. Thin section porosity within Microfacies 4 and 6 is interparticle in nature and comprises between 4-10% of the rock. In Microfacies 5, porosity ranges from 0-6% and is predominantly interparticle and moldic. Porosity of Microfacies 11 is reduced by poikilotopic cement (Fig. 14E) and equant spar resulting in low intercrystalline porosities (1%). Beds near the tops of outcrops have no trace of cements (Fig. 14F) and are highly porous (~20%). These dolostones lack significant cement. Dolomite crystals are euhedral without any evidence of leaching. Calcite cements present in dolostones directly beneath these rocks also display minimal solution features. Interparticle and fracture porosity are locally present throughout all samples and contribute to overall porosity. Porosity of Microfacies 7 is mostly due to late-stage fracturing and ranges from 0-7%. Microfacies 1, 8, and 9 are the least porous microfacies with an average of less than 1%. Most of this porosity is due to fracturing. Siltstones of Microfacies 3 and 10 have a porosity range of 0-15% depending upon the amount of fracturing and preserved interparticle porosity. Fractures, molds, vugs, and interparticle porosity are the main types of porosity within Microfacies 2. Porosity ranges from 0-8%.

Core Plug Porosity/Permeability

Measured porosities and permeabilities are plotted together with porosity on the x-axis and permeability on a log-normalized y-axis (Fig. 15). Samples were grouped according to the unit in which they occurred; lower limestone, middle clastic, and upper dolostone. Measured porosities from core plugs range from 1-23% and permeabilities

from 0-279 mD. Porosities within the lower and middle units (Association A and B) of the Sinbad Limestone are variable and range from 1-12%. Porosity within these units is greatly reduced by pore-filling spar and internal sediment. In some of the more porous areas, porosity is enhanced by dissolution of carbonate material to form vugs. Primary interparticle porosity is also preserved in some beds. Permeabilities are generally low and range from 0-0.01 mD. High permeabilities in the lower and middle units are related to fracturing.

Dolostones of the upper unit (Association C) can be separated into two basic categories: those with high porosity/permeability and those with low porosity/permeability. Low porosity/permeability dolostones have ranges very similar to

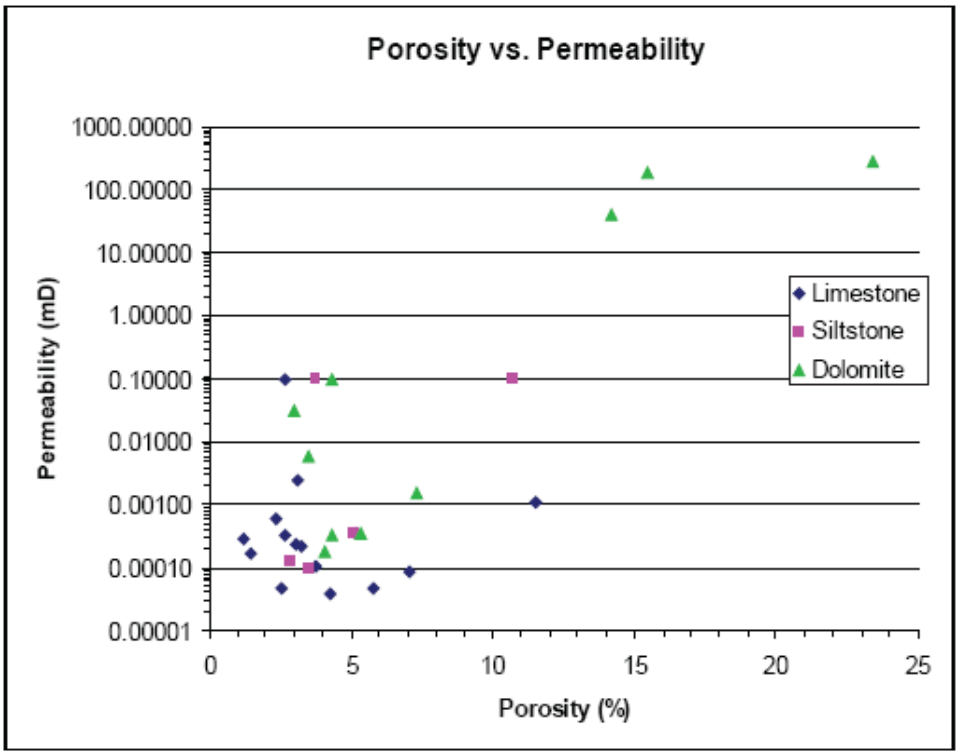

Figure 15. Crossplot of porosity and permeability measurements obtained from the Spotted Wolf panel.

underlying rocks for the same reason, cementation. Dolostones with high intercrystalline porosity and permeability have porosity values above 15% and permeabilities ranging from 10-279 mD.

Reservoir Characterization

Through analysis of porosity and permeability, reservoir characterization of the Sinbad Limestone is possible. Low porosity is characteristic of Microfacies 1. However, due to the limited lateral extent of this microfacies, it is unlikely to be a major barrier within the Sinbad reservoir. Bioturbated beds of Microfacies 3 have been bioturbated and altered in such a way that all primary porosity and permeability has been destroyed. Beds of Association A often contain oil within non-touching pore spaces (Fig. 14D). One of the microfacies with the largest amount of oil is Microfacies 2. As stated above, of 10 thin sections, eight contain dehydrated oil in interparticle and vuggy porosity. Low porosities and permeabilities due to diagenetic alteration constrain these units to storing oil rather than producing it. Hardgrounds are often associated with fibrous marine cement, encrusting organisms and laminated silt. They have little porosity or permeability and likely either serve to partition the reservoir and in the case of the lowermost hardground, act as important barriers to the flow of oil.

Coupled with the restriction of oil to the lower limestone units is the baffle/barrier nature of Association B as well as several beds of siltstone within Association A. Low porosities and permeabilitites due to the fineness of the sediment and the dominance of calcite cement have the effect of restricting or even stopping the flow of oil.

Most beds within Association C have been highly dolomitized and cemented and show little potential of serving as reservoirs. High porosities and permeabilities (Fig. 15)

within several of the dolostone beds show a large potential of acting as flow units; little to no cement is present to restrict the flow of fluids. These beds are quite thin (~1 m) compared to the rest of the Sinbad Limestone and as such are relatively small targets for oil. Gas could potentially be exploited from these beds, however. Most of the microfacies studied show low porosity and permeability. What little permeability there is has been enhanced by fracturing. If the Sinbad Limestone is going to produce oil, interconnectivity between the oil storage units of Association A and oil flow units of Association C must be established.

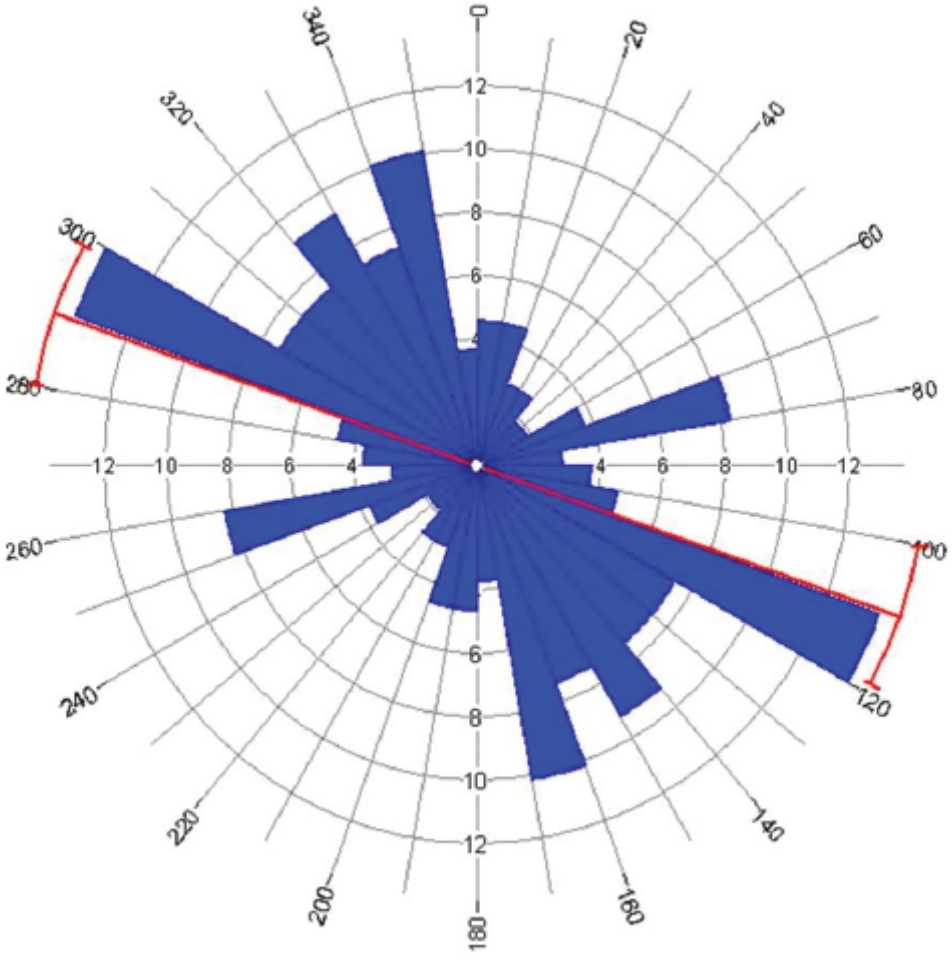

Figure 16. Rose diagram of measured fracture orientations. N = 110.

Fractures

Because of the low permeability and porosity of producing units, Lutz and Allison (1992) concluded that fractures are critical to production in the Grassy Trail Creek Field. From the above discussion of the low porosity and permeability, it is concluded that fracturing is an important characteristic of the Sinbad Limestone. Any characterization of this rock unit would be incomplete without fracture analysis.

Sampling problems related to the width of the well bore and to the spacing of adjacent wells represent a fundamental challenge to subsurface fracture characterization (Ortega et al., 2006). The traditional approach for predicting the abundance of subsurface fractures is to understand how geological parameters (such as rock type, bed thickness, etc.) control variations in fracture intensity. Core studies show that fracture intensity patterns evolve with progressive diagenesis (Marin et al., 1993) and that lower porosity rocks of similar composition should have more abundant fractures than higher porosity rocks (Nelson, 2001).

Orientation of fractures was obtained using a Brunton compass from all three localities mentioned above. A rose diagram of these data is located in Fig 16. As can be seen from this figure, there is a strong NW-SE orientation of fractures. Secondary peaks are oriented more northerly, and almost opposite of the strongest peak. A NW-SE orientation of fractures corresponds well with published accounts of fracture orientation in the area as well as the secondary NE-SW direction (Delaney and Gartner, 1997; Bump and Davis, 2003, and Davatzes et al., 2003)

To develop a model to predict fracture intensity (number of fractures per unit length along a scan line) in the subsurface, data were collected on spacing, width, relative

length, and orientation of fractures in three surface sections: Fracture localities 1 and 2, and the Spotted Wolf section (Fig. 1). Scan lines were chosen to represent contrasting sedimentary rock types and bed thicknesses. Aperture size was measured using the fracture-aperture comparator of Ortega et al. (2006). If apertures were larger than 5 mm they were measured with a standard tape measure. Calculation of fracture intensity was normalized using methods of cumulative-frequency fracture size distributions described by Orgeta et al. (2006). Cumulative frequency is calculated as 1/S. Fracture apertures and cumulative fracture intensity were then plotted on a scatter plot using Microsoft Excel. One point is equal to one normalized fracture. Logarithmic best-fit lines were fitted to the data. The equation and R^2-value of the best-fit line are given in Figure 17.

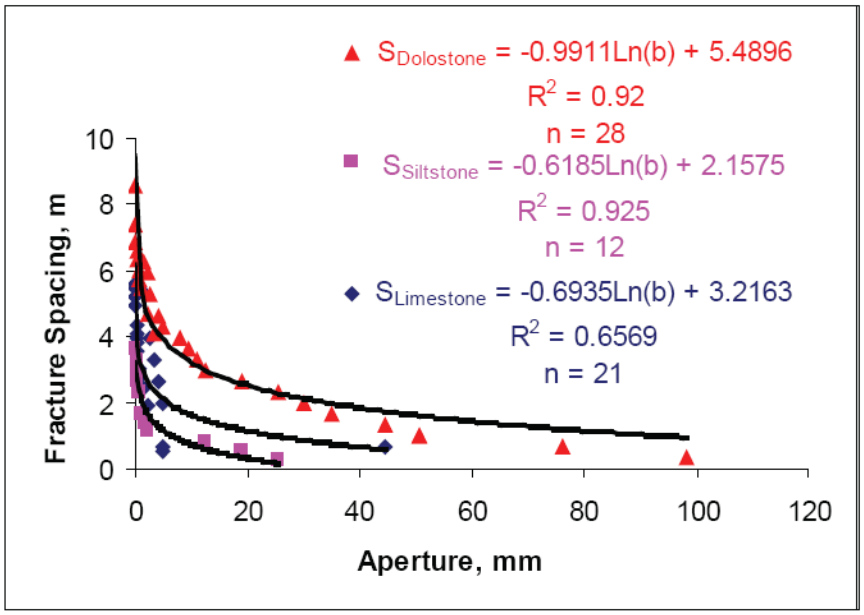

Figure 17. Normalized fracture intensity from cumulative fracture-size distribution for fractures in the three lithofacies within the Sinbad Limestone. In the best-fit equations, b = aperture, and S = fracture spacing.

As evident from this graph, fracture spacing is different with all three different lithologies with spacing being largest in dolostones and smallest in the siltstones. The

R^2-value for dolostone and siltstone are both high; however, the R^2-value for limestone is relatively low (Fig. 17). This is possibly because of a higher dependence on bed thickness or microfacies type in limestones to determine fracture spacing. When bed thickness and microfacies type are allowed to remain constant, the R^2-value is much higher (18A, B, C). It is also interesting to note that the degree of dolomitization contributes to fracture spacing, i.e. fracture spacing increases with dolomitization. Large-aperture fractures are more likely to be conductive than low-aperture fractures (Ortega, 2006). Using this information, it is possible to predict the necessary fracture orientation and drilling length to come into contact with the necessary fractures to produce the maximum amount possible.

CONCLUSIONS

The Sinbad Limestone Member of the Moenkopi Formation is a thin, mixed carbonate/siliciclastic interval with reservoir potential throughout much of central Utah. The Sinbad Limestone represents two parasequences deposited on a shallow storm-dominated ramp. Three units are present within the Sinbad Limestone: a basal well-circulated limestone, a middle restricted siltstone, and an upper dolomitized oolite shoal.

Analysis of samples from the Sinbad Limestone results in 11 microfacies. Microfacies 1 is characterized by building of stromatolites and filling of accommodation space. Microfacies 2, 4, 5, 6, 7, 8, and 9 are carbonate sediments of Association A that show influence of storm deposition. Microfacies 3 represents time in between storms where infauna are able to burrow and bioturbated the sediments. Also found with Association A are transgressive silts of Microfacies 10. Association B is composed of lagoonal-type sediments of Microfacies 10 that are the result of restriction of waters on

the ramp and a decrease in biotics. Dolomitized ooids of Microfacies 11 represent deposition from tidally-influenced ooid shoals of Association C.

Diagenesis is ubiquitous throughout the Sinbad Limestone and appears to be strongly controlled by microfacies association. Limestones of Association A show micritization, fibrous isopachous cements, neomorphism of molluscan grains, equant and drusy spar, and fracturing. Association B has euhedral dolomite rhombs, silica and calcite cementation, pressure solution, and fracturing. Ooids of Association C are micritized, dolomitized, and compacted. They are also cemented by poikilotopic calcite cement. Diagenetic trends show evidence of marine phreatic environments followed by meteoric phreatic environments, and finally of burial. Diagenesis within the Sinbad Limestone has effectively reduced or destroyed primary porosity, while being enhanced by minor dissolution and fracturing.

Porosity and permeability are correlated to depositional lithofacies. Porosity and permeability within the lower limestone unit and middle siliciclastic unit are extremely low with small increases reflective of fracturing. Porosity and permeability of the upper dolostone cap are reflective of the presence/absence of poikilotopic calcite cement. Where this cement is present, little to no porosity or permeability exist; however, where absent, large porosities/permeabilities are present.

Basal limestone units are oil storage units, siltstones are baffles/barriers to oil flow, and dolostone caprocks are oil flow units. If good connectivity through fractures can be obtained of the dolostone and limestone units, the Sinbad Limestone has good potential of serving as a reservoir. Fractures have a strong NW-SE trend with a smaller peak directed almost opposite of this trend. Fracture spacing increases with degree of

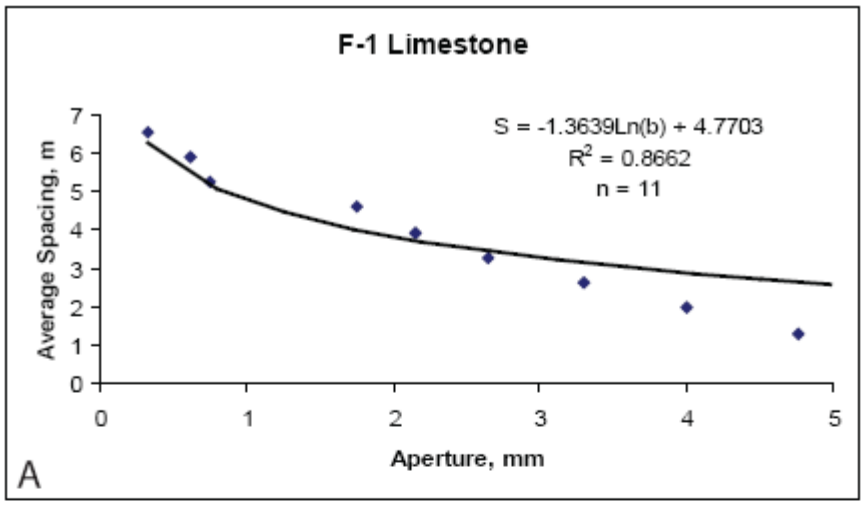

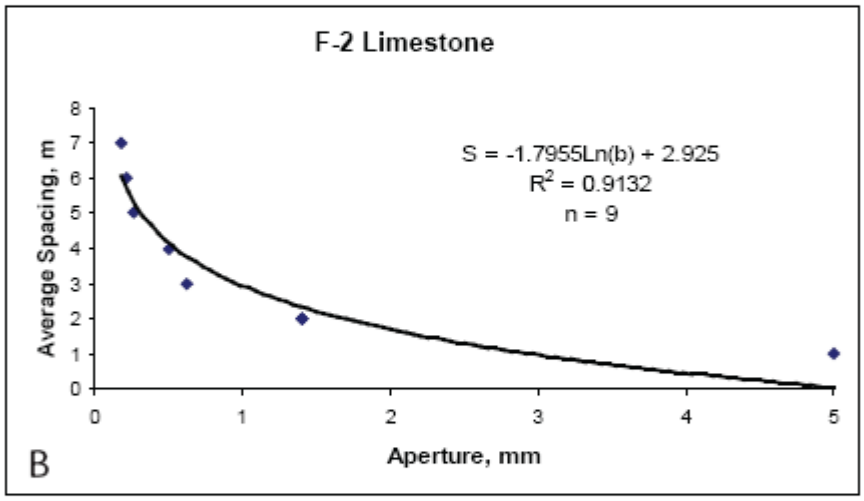

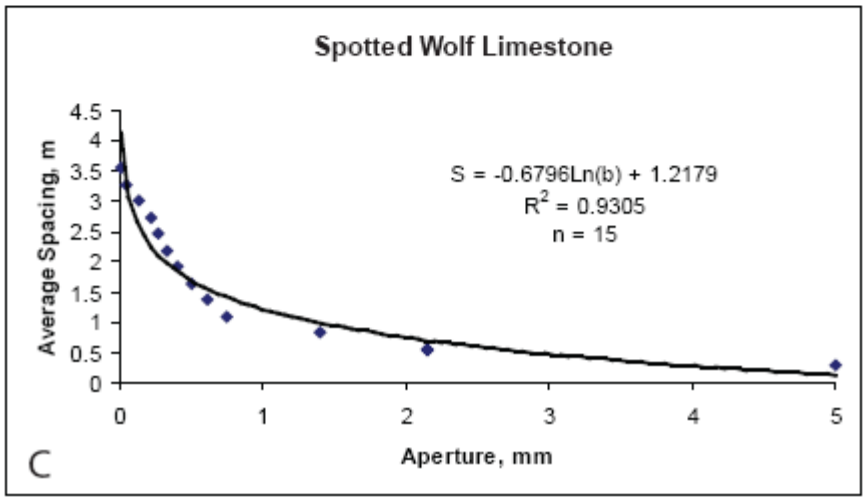

Figure 18. Normalized fracture intensity from cumulative fracture-size distribution for fractures within the Sinbad Limestone. A) Fractures from F-1 locality limestone taken from a single bed and microfacies. B) Fractures from F-2 locality limestone taken from a single bed thickness and microfacies. C) Fractures from Spotted Wolf limestone bed showing one thickness and one microfacies. S=average spacing, and b = aperture. Note: Scale differs from Figure 17 due to size of measured fractures in these three sections.

dolomitization and decreases in terrigenous sediments. In limestones, fracture spacing is possibly influenced by bed thickness and microfacies type.

REFERENCES

Allison, M.L., Lutz, S. J., and Mitchell, G.C., 1993, Grassy Trail: *In* Hill, B.G. and S.R. Bereskin (eds.), Oil and Gas Fields of Utah, Utah Geological Association Publication 22, 3 pp.

Batten, R.L., and Stokes, W.L., 1986, Early Triassic gastropods from the Sinbad Member of the Moenkopi Formation, San Rafael Swell, Utah: American Museum Novitates, v. 2864, p. 1-33.

Boyer, D.L., Bottjer, D.J., and Droser, M.L., 2004, Ecological signature of Lower Triassic shell beds of the western United States: Palaios, v. 19, p. 372-380.

Blakey, R.C., 1973a, Stratigraphy and origin of the Moenkopi Formation (Triassic) of southeastern Utah: The Mountain Geologist, v. 10, p. 1-17.

Blakey, R.C., 1973b, Stratigraphic and depositional analysis of the Moenkopi Formation, southeastern Utah: Utah Geological and Mineralogical Survey Bulletin, v. 104, 81 pp.

Blakey, R.C., 1974, Shoreline and near shore marine carbonate deposition in the Sinbad Limestone Member of the Moenkopi Formation: Geological Society of America Abstracts with Programs, v. 6, 5, p. 426.

Bump, A.E., and Davis, G.H., 2003, Late Cretaceous-Early Tertiary Laramide deformation of the northern Colorado Plateau, Utah and Colorado: Journal of Structural Geology, v. 25 p. 421-440.

Choquette, P.W. and Pray, L.C., 1970, Geologic nomenclature and classification of porosity in sedimentary carbonates: American Association of Petroleum Geologists Bulletin, v. 54, p. 207-250.

Davatzes, N.C., Aydin, A., and Eichhubl, P., 2003, Overprinting faulting mechanisms during the development of multiple fault sets in sandstone, Chimney Rock fault array, Utah, USA: Tectonophysics, v. 363, p. 1-18.

Dean, J.S., 1981, Carbonate petrology and depositional environments of the Sinbad Limestone Member of the Moenkopi Formation in the Teasdale Dome area, Wayne and Garfield Counties, Utah: Brigham Young University Geology Series, v. 28, p. 19-51.

Delaney, P.T. and Gartner, A.E., 1997, Physical processes of shallow dike emplacement near the San Rafael Swell, Utah: GSA Bulletin, v. 109, p. 1177-1192.

Dott, R.H., Jr., 1964, Wacke, graywacke, and matrix-What approach to immature sandstone classification: Journal of Sedimentary Petrology, v. 34, p. 625-632.

Dott, R.H., Jr., and Bourgeois, J., 1982, Hummocky stratification: significance of its variable bedding sequences: GSA Bulletin, v. 93, 663-680.

Dunham, R.J., 1962, Classification of carbonate rocks according to depositional texture: *In* Ham , W.E., (ed.), Classification of carbonate rocks. American Association of Petroleum Geologists Memoir 1, p. 108-121.

Ehrenberg, S.N., Nielsen, E., Svana, T.A., and Stemmerik, L., 1998, Depositional evolution of the Finnmark carbonate platform, Barents Sea: results from wells 7128/6-1 and 7128/4-1: Norsk Geologisk Tidsskrift, v. 78, p. 185-224.

Ekdale, A.A., Ekdale, S.F., and Wilson, J.L., 1976, Numerical analysis of carbonate microfacies in the Cupido Limestone (Neocomian-Aptian), Coahuila, Mexico: Journal of Sedimentary Petrology, v. 46, p. 362-368.

Folk, R.B., 1974, The natural history of crystalline calcium carbonate: Effect of magnesium content and salinity: Journal of Sedimentary Petrology, v. 44, p. 40-53.

Fraiser, M.L., and Bottjer, D.J., 2000, The U-shaped trace fossil *Arenicolites*: Burrow of an opportunist during the biotic recovery from the end-Permian mass extinction: Geological Society of America Abstracts with Programs, v. 32, 7, p. 368.

Fraiser, M.L., and Bottjer, D.J., 2004, The non-actualistic Early Triassic gastropod fauna: A case study of the Lower Triassic Sinbad Limestone member: Palaios, v. 19, p. 259-275.

Gilluly, J. and Reeside, J. B., 1928, Sedimentary rocks of the San Rafael Swell and some adjacent areas in eastern Utah: U.S. Geological Survey Professional Paper 150-D, p. 61-110.

Goodspeed, T.H., and Elrick, M., 1993, Sequence stratigraphy of the Lower Triassic Sinbad Formation, San Rafael Swell, East-Central, Utah: Geological Society of America Abstracts with Programs, v. 25, 5, p. 43.

Hammer, O., Harper, D.A.T., and Ryan, P.D. 2001, PAST: Paleontological statistics software package for education and data analysis: Palaeontologica Electronica, v. 4, p. 1-9.

Hammer, O., and Harper, D.A.T., 2005, Paleontological Data Analysis: Chichester, UK, John Wiley & Sons, 351 pp.

Hautmann, M. and Nutzel, A., 2005, First record of a heterodont bivalve (Mollusca) from

the Early Triassic: Palaeoecological significance and implications for the 'Lazarus Problem': Palaeontology, v. 48, p. 1131-1138.

Hawley, C.C., Robeck, R.C., and Dyer, H.B., 1968, Geology, altered rocks and ore deposits of the San Rafael Swell, Emery County, Utah: U.S. Geological Survey Bulletin 1239, 115 pp.

Heckel, P.H., 1983, Diagenetic model for carbonate rocks in mid-continent Pennsylvanian eustatic cyclothems: Journal of Sedimentary Petrology, v. 53, p. 733-759.

Hunt, C.B., 1953, Geology and geography of the Henry Mountains region, Utah: U.S. Geological Survery Professional Paper 228, 234 pp.

Jackson, A.L., 1993, Last Chance, South: *In* Hill, B.G. and S.R. Bereskin (eds.), Oil and Gas Fields of Utah, Utah Geological Association Publication 22, 6 pp.

Laine, M.D., and Staley, D., 1991, Summary of oil and gas exploration and production in Carbon, Emery and Sanpete Counties, East-Central Utah: *In* Chidsey, T. C. Jr. (ed.), Geology of East-Central Utah, Utah Geological Association Publication 19, p. 227-235.

Logan, B.W., Rezaki, R., and Ginsburg, R.W., 1964, Classification and environmental significance of algal stromatolites: Journal of Geology, v. 72, p. 68-83.

Lonoy, A., 2006, Making sense of carbonate pore systems: American Association of Petroleum Geologists Bulletin, v. 90, p. 1381-1405.

Lucia, F.J., 1995, Rock-fabric/petrophysical classification of carbonate pore space for reservoir characterization: American Association of Petroleum Geologists Bulletin, v. 39, p. 1275-1300.

Lutz, S. J., 1993, Sequence stratigraphic interpretation of a mixed carbonate-siliciclastic shelf environment: The Triassic Moenkopi Formation in central Utah: American Association of Petroleum Geologists Bulletin, v. 77, p. 1454.

Lutz, S. J., and Allison, M.L., 1992, Geology of the Grassy Trail Creek Field, Carbon and Emery counties, Utah: Utah Geological Survey Contract Report 92-3, 36 pp.

Marin, B.A., J.S. Clift, H.S. Hamlin, and S.E. Laubach, 1993, Natural fractures in Sonora Canyon sandstones, Sonora and Sawyer fields, Sutton County, Texas. *In* Rocky mountain Regional Meeting Lower Permeability Reservoirs Symposium. Society of Petroleum Engineers, SPE Paper #25895, p. 523-531.

McBride, E.F., 1989, Quartz cement in sandstones: A review: Earth-Science Reviews, v. 26, p. 69-112.

Nelson, R.A., 2001, Geologic analysis of naturally fractured reservoirs: Gulf Professional Publishing, 332 pp.

Nutzel, A., and Schulbert, C., 2005, Facies of two important Early Triassic gastropod lagerstatten: Implications for diversity patterns in the aftermath of the end-Permian mass extinction: Facies, v. 51, p. 480-500.

Ortega, O.J., Marrett, R.A., and Laubach, S.E., 2006, A scale-independent approach to fracture intensity and average spacing measurement: American Association of Petroleum Geologists Bulletin, v. 90, p.193-208.

Porter, M.L., 1991, Sequence stratigraphic framework of arid basin deposits: Examples from the Triassic and Jurassic of the San Rafael Swell and adjacent areas, east-central Utah: Geological Society of America Abstracts with Programs, v. 23, 2, p. 90.

Railsback, L.B., 1993, Lithologic controls on morphology of pressure-dissolution surfaces (stylolites and dissolution seams) in Paleozoic carbonate rocks from the mideastern United States: Journal of Sedimentary Petrology, v. 63, p. 513-522.

Scholle, P.A., and Ulmer-Scholle, D.S., 2003, A color guide to the petrography of carbonate rocks: Grains, textures, porosity, diagenesis: AAPG Memoir No.77., 474 pp.

Schubert, J.K., and Bottjer, D.J., 1995, Aftermath of the Permian-Triassic mass extinction event: Paleoecology of Lower Triassic carbonates in the western USA: Palaeogeography, Palaeoclimatology, Palaeoecology, v. 116, p. 1-39.

Smith, J.F., Huiff, L.C., Hinrichs, E.N., and Leudke, R.B., 1963, Geology of the Capitol Reef area, Wayne and Garfield Counties, Utah: U.S. Geological Survey Professional Paper 363, 102 pp.

Stewart, J.H., Poole, F.B., and Wilson, R.F., 1972, Stratigraphy and origin of the Triassic Moenkopi Formation and related strata in the Colorado Plateau region: U.S. Geological Survey Professional Paper 691, 195 pp.

Tucker, M.E., and Wright, V.P. 1990, Carbonate sedimentology: Malden MA, Blackwell Publishing, 482 pp.

Twitchett, R.J., Feinberg, J.M., O'Connor, D.D., Alvarez, W., and McCollum, L.B., 2005, Early Triassic Ophiuroids: Their paleoecology, taphonomy, and distribution: Palaios, v. 20, p. 213-223.

APPENDIX

Section	Name	Location
1.	JA-1	SW ¼, NE ¼, section 1, T. 22 S, R. 12 E
2.	JA-2	SW ¼, NE ¼, section 31, T. 21 S, R. 13 E
3.	JA-3	SE ¼, SE ¼, section 31, T. 21 S, R. 13 E
4.	JA-4	NW ¼, SE ¼, section 32, T. 21 S, R. 13 E
5.	JA-5	NE ¼, NW ¼, section 32, T. 21 S, R. 13 E
6.	JA-6	SE ¼, NE ¼, section 28, T. 21 S, R. 13 E
7.	JA-7	NE ¼, SW ¼, section 20, T. 21 S, R. 13 E
8.	JA-8	NE ¼, SW ¼, section 20, T. 21 S, R. 13 E
9.	JA-9	NE ¼, SW ¼, section 20, T. 21 S, R. 13 E
10.	JA-10	NW ¼, SW ¼, section 20, T. 21 S, R. 13 E
11.	JA-11	NW ¼, SW ¼, section 20, T. 21 S, R. 13 E
12.	JA-12	SE ¼, SE ¼, section 20, T. 21 S, R. 13 E
13.	JA-13	NE ¼, NE ¼, section 29, T. 21 S, R. 13 E
14.	Spotted Wolf	SE ¼, NE ¼, section 3, T. 22 S, R. 13 E
F-1.	Fracture Locality 1	NW ¼, SE ¼ section 9, T. 21 S, R. 11 E
F-2.	Fracture Locality 2	SE ¼, NW ¼ section 24, T. 22 S, R. 11 E